frontiers | Frontiers in Marine Science

TYPE Original Research
PUBLISHED 29 August 2022
DOI 10.3389/fmars.2022.954059

OPEN ACCESS

EDITED BY
Martin F. Soto-Jimenez,
Institute of Marine Science and Limnology, National Autonomous University of Mexico, Mexico

REVIEWED BY
Koji Sugie,
Japan Agency for Marine-Earth Science and Technology (JAMSTEC), Japan
Chengyan Liu,
Southern Marine Science and Engineering Guangdong Laboratory, China

*CORRESPONDENCE
Gianmarco Ingrosso
gianmarco.ingrosso@isp.cnr.it
Michele Giani
mgiani@ogs.it

SPECIALTY SECTION
This article was submitted to Marine Biogeochemistry, a section of the journal Frontiers in Marine Science

RECEIVED 26 May 2022
ACCEPTED 03 August 2022
PUBLISHED 29 August 2022

CITATION
Ingrosso G, Giani M, Kralj M, Comici C, Rivaro P, Budillon G, Castagno P, Zoccarato L and Celussi M (2022) Physical and biological controls on anthropogenic CO_2 sink of the Ross Sea. *Front. Mar. Sci.* 9:954059. doi: 10.3389/fmars.2022.954059

Physical and biological controls on anthropogenic CO_2 sink of the Ross Sea

Gianmarco Ingrosso[1,2*], Michele Giani[2*], Martina Kralj[2], Cinzia Comici[2], Paola Rivaro[3], Giorgio Budillon[4], Pasquale Castagno[5], Luca Zoccarato[6] and Mauro Celussi[2]

[1]Institute of Polar Sciences (ISP), National Research Council (CNR), Bologna, Italy, [2]Oceanography Division, National Institute of Oceanography and Applied Geophysics – OGS, Trieste, Italy, [3]Department of Chemistry and Industrial Chemistry, University of Genova, Genova, Italy, [4]Department of Science and Technology, University of Naples "Parthenope", Naples, Italy, [5]Department of Mathematics, Computer Sciences, Physics, and Earth Sciences, University of Messina, Messina, Italy, [6]Department of Plankton and Microbial Ecology, Leibniz Institute of Freshwater Ecology and Inland Fisheries (IGB), Stechlin, Germany

The Antarctic continental shelf is known as a critical anthropogenic CO_2 (C_{ant}) sink due to its cold waters, high primary productivity, and unique circulation, which allow it to sequester large amounts of organic and inorganic carbon into the deep ocean. However, climate change is currently causing significant alteration to the Antarctic marine carbon cycle, with unknown consequences on the C_{ant} uptake capacity, making model-based estimates of future ocean acidification of polar regions highly uncertain. Here, we investigated the marine carbonate system in the Ross Sea in order to assess the current anthropogenic carbon content and how physical–biological processes can control the C_{ant} sequestration along the shelf-slope continuum. The Winter Water mass generated from convective events was characterized by high C_{ant} level (28 μmol kg^{-1}) as a consequence of the mixed layer break-up during the cold season, whereas old and less-ventilated Circumpolar Deep Water entering the Ross Sea revealed a very scarce contribution of anthropogenic carbon (7 μmol kg^{-1}). The C_{ant} concentration was also different between polynya areas and the shelf break, as a result of their specific hydrographic characteristics and biological processes: surface waters of the Ross Sea and Terra Nova Bay polynyas served as strong CO_2 sink (up to –185 mmol m^{-2}), due to the remarkable net community production, estimated from the summertime surface-dissolved inorganic carbon deficit. However, a large amount of the generated particulate organic carbon was promptly consumed by intense microbial activity, giving back carbon dioxide into the intermediate and deep layers of the continental shelf zone. Further C_{ant} also derived from High-Salinity Shelf Water produced during winter sea ice formation (25 μmol kg^{-1}), fueling dense shelf waters with additional input of C_{ant}, which was finally stored into the abyssal sink through continental slope outflow (19 μmol kg^{-1}). Our results suggest that summer biological activity over the Ross Sea shelf is pivotal for the shunt of anthropogenic CO_2 between the organic and inorganic carbon pools,

enhancing the ocean acidification of the upper mesopelagic zone and the long-term C_{ant} sequestration into the deep ocean.

KEYWORDS

anthropogenic CO_2, carbonate system, ocean acidification, Ross Sea, Antarctica

Introduction

The Southern Ocean plays a crucial role in regulating the Earth's climate by absorbing approximately 30%–40% of the global oceanic uptake of anthropogenic CO_2 (C_{ant}) (Sabine et al., 2004; Gruber et al., 2009; Khatiwala et al., 2013). An important component of this uptake occurs in Antarctica's continental shelves and coastal polynyas (Arrigo et al., 2008a), where high primary production and formation of Dense Shelf Water (DSW) have the potential to efficiently sequester the C_{ant} into the deep ocean over centennial time scales (Sigman et al., 2010). However, notable discrepancies exist among different Antarctic shelf areas (Arrigo et al., 2008b; Lee et al., 2017), and regional estimates of net CO_2 uptake (Mahieu et al., 2020) come with large uncertainties (McKinley et al., 2017; Gruber et al., 2019). This limited knowledge is mostly due to sparse observations (Lenton et al., 2013) and incomplete evaluations of the different processes that govern the ocean carbon dynamics, such as melt water influence, sea surface temperature, ocean circulation, wind regimes, and biological processes (Takahashi et al., 2012). Furthermore, the amount of C_{ant} that is buried into local shelf sediments, recycled into the water column, and exported elsewhere into the deep ocean is still not well quantified.

The Ross Sea is among the most biologically productive areas of the Southern Ocean (Arrigo and McClain, 1994; Smith and Gordon, 1997; Arrigo et al., 2008b) and an important site of dense water formation (Jacobs et al., 1970; Orsi et al., 1999), making this particular region a large CO_2 sink on an annual scale (Arrigo et al., 2008a). The CO_2 drawdown capacity of the Ross Sea is particularly prominent on the western side, which hosts two large polynyas (i.e., areas of open waters or reduced sea ice cover surrounded by higher concentrations of ice), namely the Ross Sea polynya and Terra Nova Bay polynya, with massive phytoplankton blooms and intense production of dense shelf waters. During winter, the Ross Sea is mostly covered in sea ice. Microalgae start to bloom in October when sea ice usually breaks up in the central region (Smith and Gordon, 1997; Smith et al., 2000; Arrigo and van Dijken, 2004; Arrigo et al., 2015). During November, the sea ice-free areas expand and primary production increases abruptly. Maximum primary production occurs in late spring (December) and decreases sharply in summer (January and February) due to iron limitation (Fitzwater et al., 2000; Sedwick et al., 2000; Coale et al., 2005; Sedwick et al., 2011) as well as light limitation and deep vertical mixing at the beginning of the winter season (Nelson and Smith, 1991; Sakshaug et al., 1991; Saggiomo et al., 2002). Sea ice re-forms quickly in early March and continues to expand throughout winter. Brine is rejected during sea ice production, which subsequently sinks and helps to generate saline-dense shelf waters (Budillon et al., 2003; Orsi and Wiederwohl, 2009). Strong and cold katabatic winds that flow from land over the ocean promote the development of the polynyas by enhancing intense sea ice growth that is constantly pushed away from the shore, thus sustaining areas of open water or thin ice for much of the year (Williams et al., 2007).

Net community production (NCP), defined as gross primary production minus community respiration, changes the pCO_2 of surface water and thereby the seasonal air–sea CO_2 flux in coastal polynyas. The Ross Sea atmospheric carbon uptake is largely controlled by NCP and carbon export to the deep layers of the water column. DeJong et al. (2017) found an outstanding net community production (-425 ± 204 mmol C m^{-2} day^{-1}) during the late summer in Terra Nova Bay (TNB), which was rapidly exported below 200 m depth. Arrigo et al. (2000) also found that between 70% and 100% of NCP was present as particulate organic carbon (POC) in the upper 150 m during a mid-December through early January cruise. The summer POC standing stock production, remineralization, and export influence the magnitude of the Ross Sea anthropogenic carbon sink. Furthermore, dense water formation events are key processes that govern outstanding events of C_{ant} uptake from the atmosphere and its subsequent storing into the deep ocean. During winter, very low seawater temperatures and associated katabatic winds can lead to CO_2 uptake of up to −250 mmol C m^{-2} day^{-1}, as found by DeJong and Dunbar (2017) in TNB. Intense sea-ice formation and brine rejection drive the DSW to flow down along the continental slope and to produce Antarctic Bottom Water (AABW), which ultimately supplies atmospheric CO_2 to the deeper layers of the Southern Ocean and thus determining its long-term sequestration.

Due to the complexity of the processes involved, little is known about the current C_{ant} content in the Ross Sea and how physical and biological processes control the transport and fate of carbon dioxide from the atmosphere to the deep ocean. Here

we present the summer CO_2 system in the Ross Sea, estimated by discrete water samples of total alkalinity (TA) and pH. These new observations are used to assess the present C_{ant} concentration and to evaluate its long-term temporal change in the region. Additionally, we combine measurements of microbial metabolic activity, POC standing stock, and net community production *via* seasonal deficit in total inorganic carbon to highlight the importance of both physical and biological processes in controlling the anthropogenic CO_2 levels, sequestration, and export.

Oceanographic setting

We follow the water mass characterization of Orsi and Wiederwohl (2009) to define the main water masses in the Ross Sea during the summer season, considering potential temperature (θ), salinity (S), and neutral density (γ^n) (see Table 1; Figure 2). Antarctic Surface Water (AASW) is the lightest water mass (γ^n< 28.00 kg m^{-3}) and is characterized by highly variable temperatures and salinities due to the seasonal influence of sea ice formation and melting. Circumpolar Deep Water (CDW) is a relatively warm (>1°C), salty, and low-oxygenated water with a γ^n value between 28.00 and 28.27 kg m^{-3}. This water mass derives from the Antarctic Circumpolar Current and intrudes onto the shelf mostly along the western slope of the Ross Sea banks (Wang et al., 2013; Castagno et al., 2017). When CDW enters the Ross Sea, it mixes with local waters near the shelf break to form modified CDW (mCDW), which is defined by the same density range as CDW but with lower temperatures. The inflow of CDW has a great influence on the heat, salt, and nutrient budget of the continental shelves and is critical to the regional sea-ice cycle (Smith et al., 2012), basal melt rate of the Ross Ice Shelf (Rignot and Jacobs, 2002; Pritchard et al., 2012), and AABW formation (Whitworth and Orsi, 2006; Budillon et al., 2011). The water column of the shelf area is also occupied by Winter Water (WW), a cold water mass representing the remnant of the previous winter's surface mixed layer (Porter et al., 2019) and setting at a depth range that depends on its location within the polynya. The remaining classifications regard the densest water masses (γ^n > 28.27 kg m^{-3}) on the shelf and slope. Ice formation increases sea-surface salinity and produces High Salinity Shelf Water (HSSW) that presents a salinity value greater than 34.62. HSSW is formed mostly in the TNB area during winter (Budillon et al., 2003), spreads northwards following the Drygalski Basin, and finally flows off the shelf near Cape Adare, where it mixes with CDW to produce AABW (Whitworth and Orsi, 2006; Gordon et al., 2015). During the transfer towards the continental shelf break, HSSW mixes with mCDW to form Modified Shelf Water (mSW, θ > −1.85°C). Ice Shelf Water (ISW) is the last water mass denser than 28.27 kg m^{-3} and is defined by temperatures below the freezing point at 50 dbar (θ ≤ −1.95°C). This supercooled water mass is present in front of the Ross Ice Shelf at an intermediate depth and is a mixture of basal ice shelf meltwater and shelf water.

Methods

In situ data were collected onboard the R/V Italica, as part of the National Program for Research in Antarctica (PNRA). The biogeochemical parameters were investigated at 17 stations by sampling five to eight depths from surface to 1,750 m from 11 January to 04 February 2014. The position of the casts is shown in Figure 1. They were mainly in the western Ross Sea, along the Drygalski Basin (DB) from Terra Nova Bay polynya (TNBp) to the shelf break region off Cape Adare (CA); a few stations were also sampled both in the Hillary Canyon (HC) and in the Ross Sea polynya (RSp). Hydrological casts and water sampling were

TABLE 1 Estimated mean values of potential temperature (θ; °C), salinity (*S*), neutral density anomaly (γ^n; kg m^{-3}), dissolved oxygen concentration (DO; µmol kg^{-1}), total alkalinity (TA; µmol kg^{-1}), total dissolved inorganic carbon concentration (TCO_2; µmol kg^{-1}), pH_T at *in situ* temperature (pH_T *in situ*), aragonite saturation state (Ω_{ar}), anthropogenic carbon concentration (C_{ant}; µmol kg^{-1}), pH reduction from the preindustrial era (ΔpH_T), and aragonite saturation state reduction from the preindustrial era ($\Delta\Omega_{ar}$) of each water mass in the Ross Sea.

Parameter	AASW	CDW	mCDW	mSW	HSSW	ISW	WW
θ	−0.30	0.86	−0.56	−0.58	−1.91	−1.95	−1.89
S	34.16	34.71	34.57	34.66	34.75	34.66	34.70
γ^n	27.67	28.14	28.12	28.36	28.7	28.59	28.64
DO	337	199.5	243.6	238.7	281	277.1	283.2
pH_T *in situ*	8.171	7.993	8.024	8.015	8.046	8.025	8.062
TA	2,324	2,355	2,343	2,349	2,356	2,353	2,350
TCO_2	2,165	2,259	2,259	2,255	2,251	2,259	2,249
Ω_{ar}	1.7	1.1	1.2	1.1	1.1	1.1	1.2
C_{ant}		7	30	19	25	31	28
ΔpH		−0.03	−0.09	−0.06	−0.07	−0.09	−0.08
$\Delta\Omega_{ar}$		−0.09	−0.27	−0.18	−0.23	−0.29	−0.26

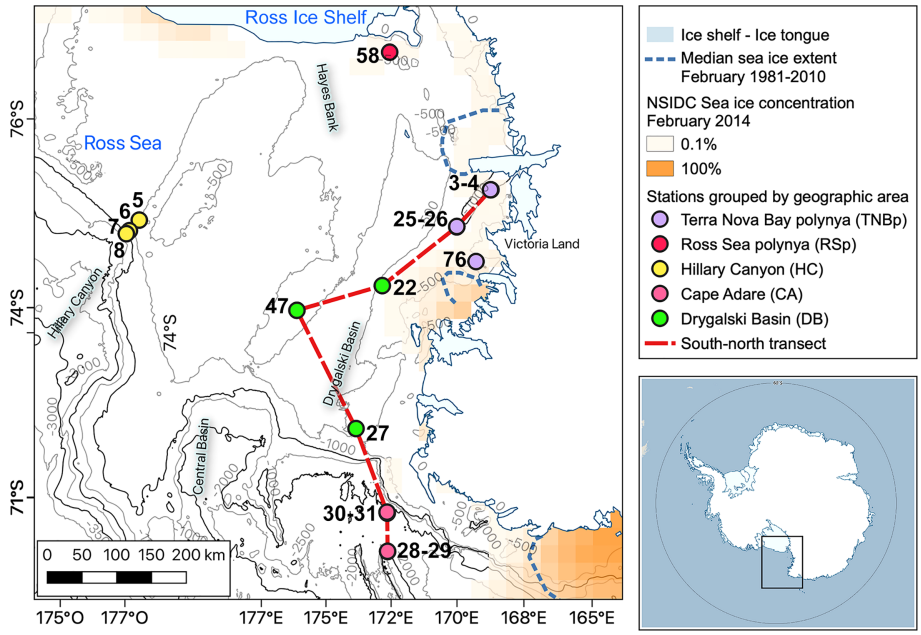

FIGURE 1
Map of the Ross Sea. Sampling stations during the XXIX Italian expedition are indicated by circles. The geographic areas in which the sampling stations are grouped are Terra Nova Bay polynya (TNBp), Ross Sea polynya (RSp), Hillary Canyon (HC), Cape Adare (CA), and Drygalski Basin (DB). Bathymetry is from Arndt et al. (2013) (IBCSO V1.0) with 500 m contour intervals (1,000, 2,000, and 3,000 m in dark lines). Polynya regions were shown using the satellite-derived sea-ice concentration during February 2014 (National Snow and Ice Data Center (NSIDC), Fetterer et al., 2017). Median extent of sea ice in February over a 20-year period (1981–2010) (dashed blue contours, Fetterer et al., 2017). Map developed from Quantarctica GIS package, Norwegian Polar Institute (Matsuoka et al., 2018).

carried out using an SBE 9/11 Plus CTD, with double temperature and conductivity sensors, coupled with an SBE 32 plastic-coated carousel sampler, on which 24 12-L Niskin bottles were mounted. The entire dataset has been indexed with the DOI 10.13120/cfeaa3ca`b9c-445f-be27-a74e346026ba and is freely available at https://nodc.ogs.it/catalogs/doidetails?4&doi=10.13120/cfeaa3ca-2b9c-445f-be27-a74e346026ba. All oceanographic analysis and their graphical representations were performed with the "OCE" package in R (Kelley, 2018) and following the colormap selection of Thyng et al. (2016).

Carbonate system

For the total alkalinity, samples were pre-filtered on glass-fiber filters (Whatman GF/F) into 500-ml narrow-necked borosilicate glass bottles and poisoned with 100 µl of saturated mercuric chloride ($HgCl_2$) to halt the biological activity, sealed with glass stoppers and stored at 4°C in the dark until analysis. Total alkalinity was determined by potentiometric titration in an open cell (SOP 3b, Dickson et al., 2007) using a nonlinear least squares approach. To approximate the ionic strength of the samples, the HCl titrant solution (0.1 mol kg^{-1}) was prepared in NaCl background and calibrated against certified reference seawater (CRM, Batch #107, provided by A.G. Dickson, Scripps Institution of Oceanography, USA). The accuracy and precision of the TA measurements on CRM were determined to be less than ± 2.0 µmol kg^{-1}. Additionally, repeated measurements ($n \geq 3$) on in-house standards of natural seawater were undertaken every day prior to sample analysis in order to monitor the instrument's accuracy and precision frequently. The pH was measured using a double-wavelength spectrophotometer (Cary 100 Scan UV-Visible) and a purified m-cresol purple indicator dye following SOP 6b of Dickson et al. (2007). The precision of the method, expressed as the standard deviation of replicates from the same Niskin bottles, was ±0.002, and pH results were reported on a total scale (pH_T). The total dissolved inorganic carbon concentration (TCO_2) and aragonite saturation (Ω_{ar}) levels were estimated by the R package Seacarb (Gattuso et al., 2015) from AT, pH_T measured at 25°C (pH_T 25°C), T, S, phosphate, and silicate data as inputs. For the first time, carbonic acid equilibrium constants (i.e., pK_1 and pK_2) of Sulpis et al. (2020) were used for the calculation of CO_2 system parameters of the Ross Sea, which represent the current most appropriate constants for the cold oceanic regions and minimize the overall uncertainty when seawater

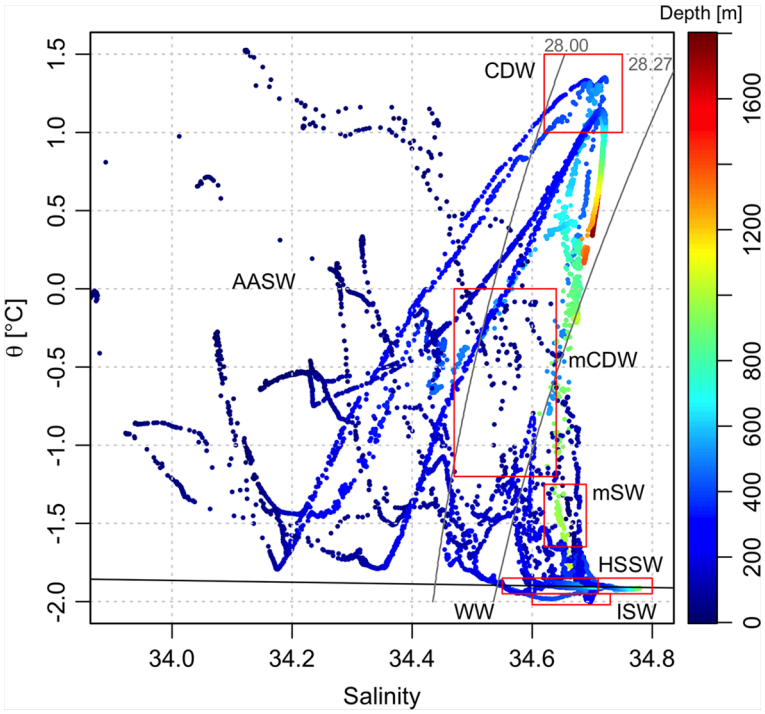

FIGURE 2
Potential temperature/salinity (θ/S) plot for the sampled stations. Grey solid lines show the 28.00 and 28.27 kg m^{-3} neutral density anomaly (γ^n). The black horizontal line shows the surface freezing point of seawater. The color scale bar refers to the sampling depth. Major water masses are labeled as follows: Antarctic Surface Water (AASW), Circumpolar Deep Water (CDW), modified Circumpolar Deep Water (mCDW), High Salinity Shelf Water (HSSW), Ice Shelf Water (ISW), modified Shelf Water (mSW), and Winter Water (WW).

temperature is below ~8° −9°C. Finally, the Dickson dissociation constant for hydrogen sulfate (Dickson, 1990) and the borate constant of Lee et al. (2010) was used.

Dissolved oxygen, nutrients, and particulate organic carbon

For the determination of dissolved oxygen (DO) concentration, the Winkler method was followed (Grasshoff, 1983) using an automated titration system (Methohm 719 titroprocessor) with potentiometric end-point detection (Oudot et al., 1988). The analytical precision and accuracy was ± 0.2 µmol kg^{-1}. Samples for dissolved inorganic nutrients were filtered on board on precombusted Whatman GF/F filters and kept frozen (−20°C) until laboratory analysis. Dissolved inorganic nutrients were determined with a segmented flow QUAATRO Seal Analytical AutoAnalyzer following standard colorimetric methods (Hansen and Koroleff, 1999). The detection limits of nutrient concentrations reported by the analytical methods are 0.02, 0.02, and 0.02 µM, respectively, for N-NO_3, P-PO_4, and Si-Si$(OH)_4$. The accuracy and precision of the analytical procedures at low concentrations were checked annually through the quality assurance program QUASIMEME and the relative coefficient of variation for five replicates was less than 5%. Internal quality control samples were used during each analysis. For the purposes of this work, nutrient data were used only for the accurate calculation of the full set of carbonate system variables, so their specific distribution patterns are not presented here.

POC and particulate nitrogen (PN) were measured using an elemental analyzer, CHNO-S Costech mod. ECS 4010, applying the methods by Pella and Colombo (1973) and Sharp (1974). Samples ranging from 1.1 to 8.0 L were filtered on 25-mm precombusted Whatman GF/F and filters and stored at −80°C. Before analysis, filters were treated with the addition of 200 µl of HCl 1N to remove the carbonate and then dried at 60°C for about 1 h with the similar method of Lorrain et al. (2003). Before the analysis, the filter was inserted into a 10 × 10-mm tin capsule. Known amounts of standard acetanilide (C_8H_9NO—Carlo Erba; assay ≥99.5%) were used to calibrate the instrument. The detection limits for PN and POC, defined as twice the standard deviation of the blank (5–10 blank 25-mm filters), were 0.01 µmol-N L^{-1} and 0.001 µmol-C L^{-1}, respectively. The relative standard deviations for three replicates of internal quality control sample replicates were lower than 10%. The

accuracy of the method was verified periodically against the certified marine sediment reference material PACS-2 (National Research Council Canada).

Prokaryotic abundance and heterotrophic metabolic rates

Samples for the assessment of prokaryotic abundance (PA) were fixed with 0.2 μm filtered formaldehyde solution (2% final concentration, f.c.; Fluka). They were stored in sterile dark bottles at 4°C and processed following Porter and Feig (1980); three analytic replicates per sample were done (3–8 ml). Aliquots of each sample were stained with a 4′,6-diamidino-2-phenylindole (DAPI) solution at 1 μg ml^{-1} final concentration and placed in the dark for 15 min. Cells were collected on 0.22 μm black polycarbonate filters (Nucleopore, 25 mm), and each filter was immediately placed on a slide between two drops of immersion nonfluorescent oil (type A, Cargille, Cedar Grove, NJ, USA) and kept at −20°C in the dark. Cell counts were made using an epifluorescence microscope (Olympus BX 60 F5) utilizing a UV filter set (BP 330–385 nm, BA 420 nm) at ×1,000 final magnification; more than 200 cells were counted.

Prokaryotic heterotrophic production (PHP) was measured by the incorporation of ^{3}H-leucine (Kirchman et al., 1985). Triplicate 1.7-ml aliquots and one killed control (5% trichloroacetic acid, f.c.; Sigma) were amended with 20 nM radiotracer (58.5 Ci $mmol^{-1}$; Perkin Elmer) and incubated for 6 h at *in situ* temperature in the dark. The extraction of ^{3}H-labeled proteins was carried out following the microcentrifugation method (Smith and Azam, 1992). The activity in the samples was determined by a TRI-CARB 2900 TR Liquid Scintillation Analyzer after the addition of 1 ml of scintillation cocktail (Ultima Gold MV; Packard).

Partitioning of seasonal changes in TCO_2 and net community production computation

Seasonal changes of TCO_2 in the summer mixed layer are driven by a combination of physical and biological processes (i.e., air–sea CO_2 exchange, mixing, sea ice melting/formation, photosynthesis, respiration, calcium carbonate precipitation, and dissolution). According to Arroyo et al. (2020), we computed the total deficit in mixed-layer TCO_2 (ΔTCO_2^{tot}; mmol m^{-2}) at each station as the depth integrated difference between an inferred winter TCO_2 concentration (TCO_2^{winter}) and the observed summer TCO_2 concentration (TCO_2^{summer}):

$$\Delta TCO_2^{tot} = \int_0^{MLD} TCO_2^{summer} - TCO_2^{winter}\, dx \qquad (1)$$

where MLD is the summer mixed layer depth, defined here as the depth at which the maximum value of the square of the buoyancy frequency (N^2) was observed (Carvalho et al., 2017). The inferred winter TCO_2 in the surface water is often estimated using the value at the temperature minimum (e.g., Bates et al., 1998; Roden et al., 2016); however, on the Antarctic shelf, this method may not be appropriate due to the presence of ISW in the marginal ice zone. We, therefore, defined the winter TCO_2 as the average concentration of all samples collected in the WW mass ($TCO_2^{winter} = 2,249 \pm 3.3$ μmol kg^{-1}), which ranged between $-1.92°C < \theta < -1.70°C$ and $27.88 < \sigma_\theta < 27.98$ kg m^{-3} and occupied the water column between 300 and 600 m depth.

The ΔTCO_2^{tot} was partitioned into physical and biological drivers following the method of previous studies (e.g., Shadwick et al., 2017; Arroyo et al., 2019) according to the equation

$$\Delta TCO_2^{tot} = \Delta TCO_2^{sal} + \Delta TCO_2^{alk} + \Delta TCO_2^{bio+gas} \qquad (2)$$

The ΔTCO_2^{sal} represents the TCO_2 seasonal variation due to changes in salinity from mixing and sea ice melting and was determined as the depth-integrated difference between observed TCO_2 and salinity-normalized TCO_2 ($nTCO_2$), normalized to an inferred winter salinity of 34.7 (mean salinity of WW).

$$\Delta TCO_2^{sal} = \int_0^{MLD} TCO_2 - nTCO_2\, dx \qquad (3)$$

The term ΔTCO_2^{alk} refers to the impact of calcium carbonate processes on TCO_2. Because $CaCO_3$ dissolution and precipitation result in a TA and TCO_2 change that follows the 2:1 ratio, we calculated the ΔTCO_2^{alk} as the depth integrated half of the difference between observed TA (TA^{summer}) and salinity-normalized TA (nTA) after correcting for nitrate (Brewer and Goldman, 1976; Jones et al., 2010)

$$\Delta TCO_2^{alk} = \int_0^{MLD} \frac{TA - nTA}{2}\, dx \qquad (4)$$

The remaining $\Delta TCO_2^{bio+gas}$ term represents the influence of biological processes and air–sea CO_2 exchange and was determined by difference. TCO_2 and TA were normalized following the conventional method that assumes a zero freshwater end-member value (Sweeney et al., 2000; Shadwick et al., 2017). This approach has been shown to overestimate nTA in the coastal Antarctic (Legge et al., 2017), but few observational data are available to accurately estimate the freshwater (meteoric or melt water) TCO_2 and TA end-members in the Ross Sea.

Although the mixed layer was generally<100 m during our cruise, the reduction in TCO_2 due to biological processes was computed from the surface to 200 m at each station to account for deeper mixing prior to the sampling event. This seasonal change in TCO_2 represents the net community production rate (NCP, mmol m^{-2} day^{-1}, the imbalance between net primary

production and heterotrophic respiration) and was computed as the depth-integrated difference between the winter salinity-normalized TCO_2 ($nTCO_2^{winter}$) and observed salinity-normalized TCO_2 over the length of the productive season (PS), starting from the onset of the algal blooming until the time of sampling in January

$$NCP = \frac{\left(\int_0^{200} nTCO_2 - nTCO_2^{winter}\, dx\right)}{PS} \quad (5)$$

The start of the PS was defined as 01 November 2013 based on the increase in monthly surface chlorophyll a concentration derived from the MODIS-Aqua satellite Level 3 product at 9-km resolution (https://oceancolor.gsfc.nasa.gov/l3/).

In addition, we calculated the surplus of POC (ΔPOC) from the prebloom condition as the depth integrated difference between observed POC concentration and inferred winter POC concentration (POC^{winter}) in the upper 200 m *via*

$$\Delta POC = \int_0^{200} POC - POC^{winter}\, dx \quad (6)$$

where POC^{winter} was defined as the average concentration of all samples collected in the WW mass ($POC^{winter} = 0.85 \pm 0.4$ μmol kg^{-1}).

Estimate of anthropogenic CO_2 and ocean acidification state

The C_{ant} cannot be measured directly, as it cannot be chemically discriminated from the bulk of dissolved inorganic carbon, and different evaluation methods have been proposed (Millero, 2007; Sabine and Tanhua, 2010). All the existing methods have different advancements as well limitations depending on the assumptions and parametrizations considered. Thus, the international scientific communities have not arrived at a consensus on which model is the most accurate to estimate the concentration of C_{ant} in the ocean. Here, we chose to apply the the TrOCA (Tracer combining Oxygen, inorganic Carbon, and total Alkalinity) developed by Touratier and Goyet (2004a) and refitted by Touratier et al. (2007). Although a few studies have suggested some limitations in the use of the TrOCA for C_{ant} quantification (Huertas et al., 2009; Yool et al., 2010), this method provided robust results in different regions of the global ocean (the Atlantic Ocean, e.g., Touratier and Goyet, 2004b; Touratier et al., 2005; Vázquez-Rodríguez et al., 2009; Ríos et al., 2010; Orselli et al., 2018; de Carvalho-Borges et al., 2018; Southern and Antarctic Ocean, e.g., Lo Monaco et al., 2005; Azouzi et al., 2009; Goyet et al., 2009; Pardo et al., 2014; Kerr et al., 2018; Lencina-Avila et al., 2018; Indian Ocean, e.g., Álvarez et al., 2009; the Mediterranean Sea, e.g., Krasakopoulou et al., 2011; Hassoun et al., 2015; Palmiéri et al., 2015) and has been successfully applied in the Ross Sea (Sandrini et al., 2007). Moreover, the TrOCA approach was used to estimate the C_{ant} mixing and export under the effect of a large variety of oceanographic processes (e.g., dense water formation (Touratier et al., 2016; Ingrosso et al., 2017; Krasakopoulou et al., 2017), across-shelf transport, and deep ocean storage (Shadwick et al., 2014), and recently Bates and Johnson (2020) has demonstrated the role of this method as a useful tracer of ocean C_{ant} changes when used at a fixed location.

Briefly, the TrOCA tracer accounts for changes in carbonate chemistry and is based on the fact that below the mixed layer, the TCO_2 concentration varies according to the decomposition of organic matter and dissolution of calcium carbonate. This conservative behavior has been shown unmaintained when water masses are influenced by an anthropogenic CO_2 contribution. Thus, combining DO, TCO_2, TA, and θ is possible to calculate the C_{ant}:

$$C_{ant} = \frac{O_2 + 1.279\left(TCO_2 - \frac{1}{2}TA\right) - e^{\left(7.511 - \left(1.087x10^{-2}\right)\theta - 7.81x10^5/TA^2\right)}}{1.279}$$

The uncertainty of the estimate is ~6 μmol kg^{-1} Touratier et al. (2007). Full details of how the TrOCA approach and C_{ant} computation were derived can be found in Touratier and Goyet (2004a) and Touratier et al. (2007). Because of the large seasonal variability in the carbon content of surface waters, due to biological processes and air–sea CO_2 exchange, the TrOCA method is not appropriate for the mixed layer, and we therefore only compute C_{ant} for depths below 200 m. In addition, below the mixed layer, our N:P ratio is very close to the Redfield ratio (16.8 ± 2.1), upon which the parametrization of the TrOCA method is based.

For further evaluation of the ocean acidification impact on the Ross Sea, we estimated the anthropogenic pH and Ω_{ar} reduction from the preindustrial era (ΔpH_T and $\Delta\Omega_{ar}$) computed on the difference between the contemporary pH and Ω_{ar} measured in our study (pH_{cont} and $\Omega_{ar\ cont}$) and their preindustrial values ($pH_{pre\text{-}ind}$ and $\Omega_{ar\ pre\text{-}ind}$):

$$\Delta pHT = pH_{cont} - pH_{pre\text{-}ind} \quad (8)$$

$$\Delta\Omega_{ar} = \Omega_{ar\ cont} - \Omega_{ar\ pre\text{-}ind} \quad (9)$$

The $pH_{pre\text{-}ind}$ and $\Omega_{ar\ pre\text{-}ind}$ were derived from the TCO_2 values subtracting the anthropogenic contribution (C_{ant}) and the original TA data, since the total alkalinity is not affected by the accumulation of the atmospheric CO_2 in seawater if there is no calcifier production and dissolution change. The resulted ΔpH and $\Delta\Omega_{ar}$ data allow us to assess whether there have been significant changes in the seawater acidification state during the time between the preindustrial (~1750) period and the time of sampling (2014).

Results

Hydrographic conditions

The hydrological properties of the water masses and their spatial distribution are displayed in the θ/S diagram (Figure 2) and the south-north section (Figure 3). AASW was relatively warm and fresh (−0.30°C ± 0.89°C and 34.16 ± 0.34, Table 1), reflecting the summer conditions of surface warming and sea ice melt. Sea surface temperature was warmer in TNBp and RSp, with values ranging from −0.68°C to 1.45°C, and cooler out of the shelf area where the minimum value of −1.78°C was observed. Out the Victoria Land coast and close to the eastern side of the Ross Sea (St. 22 and 76) minimum surface salinity (S< 33.8) was observed, suggesting a significant freshwater influence deriving from a large volume of sea ice melting. The mean concentration of DO in AASW was 337 ± 42 µmol kg^{-1}, which was very close to the saturated condition (~350 µmol kg^{-1}) considering the similar surface temperature and salinity. The greatest dissolved oxygen saturation (>100%) was observed in the TNBp area, where the DO also reached the maximum value of 435 µmol kg^{-1}, decreasing toward the outer edge of the polynya and open waters (Figure 3D). Below the mixed layer, relatively warm mCDW (−0.56°C ± 0.99°C) and cold WW (−1.89°C ± 0.06°C) occupied the intermediate depths above the shelf area. WW was predominant in front of the Ross Ice Shelf and in the TNBp, with salinity value and DO concentrations of around ~34.7 and ~285 µmol kg^{-1}, respectively, and in the depth range from −300 to −600 m, likely reflecting a significant influence of winter deep convection. The signal of warm (0.86°C ± 0.31°C), salty (34.71 ± 0.01), and low-oxygenated (199 ± 2 µmol kg^{-1}) CDW was evident offshore the eastern part of the shelf break between −300 and −1,700 m (Figures 3A–C). As CDW intrudes into the shelf area, it also delivers a source of oxygen-poor waters that decreases the mCDW content of DO below the saturation level (~68%, 244 ± 28 µmol kg^{-1}, Figure 3D). HSSW occupied the deepest layers and were only found on the shelf area and near the shelf break. Due to brine rejection associated with sea ice production and surface cooling during winter, HSSW was characterized by a salinity greater than 34.7, a potential temperature near the freezing point (−1.91°C ± 0.01° C), and a decreased value of DO (281 ± 4 µmol kg^{-1}, 77% saturation). The coldest water mass, identified at ~450 m depth, was the ISW, with potential temperatures below the freezing point (−1.95°C ± 0.03°C) and salinity of about 34.66 ± 0.05. Bottom depth outflow of mSW was predominantly traced along the slope of HC by the intermediate value of salinity (34.66 ± 0.02), potential temperature (−0.58°C ± 0.71°C), and DO (239 ± 18 µmol kg^{-1}) as a result of intense downslope mixing. The clear signal of AABW was not detected during our sampling activity.

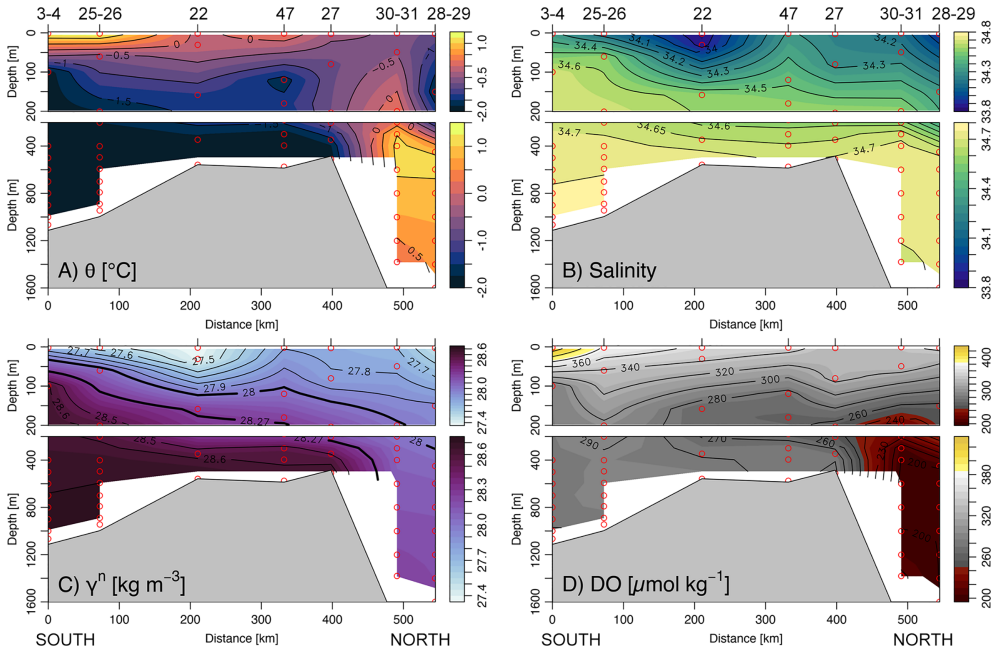

FIGURE 3
South–North vertical section across the Ross Sea (see Figure 1) for **(A)** potential temperature (θ; °C), **(B)** salinity, **(C)** neutral density anomaly (γ^n; kg m^{-3}), and **(D)** dissolved oxygen concentration (DO; µmol kg^{-1}).

CO_2 system properties

The pH_T at *in situ* temperature (pH_T *in situ*) showed the greatest values in polynya surface waters (>8.200, Figure 4A) due to warmer seawater and intense biological production. In contrast, the very low pH_T *in situ* occurred offshore and below the mixed layer (7.993 ± 0.02), coincident with the intrusion of oxygen-poor CDW. In the upper water column, TA concentration ranged from 2,274 to 2,350 µmol kg^{-1} (Figure 4B), closely resembling that of surface salinity and indicating that seasonal TA change predominantly influenced by the input of freshwater derived from summer sea ice melt. The minimum surface TCO_2 concentrations (~2,100 µmol kg^{-1}) were observed at the same locations as the salinity minimum (Figure 3C, St. 22, 27, 28–29). However, low concentrations of surface TCO_2 were also coincident with high-salinity waters, revealing the important effect of biological production in decreasing summer mixed layer TCO_2. The distribution of TCO_2 and TA with depths were similar across the considered transect, converging approximately at 300 m, in correspondence to CDW, to mean TCO_2 of 2,259 ± 1 and TA of 2,355 ± 4 µmol kg^{-1}. At a depth below 500 m, TA remained relatively constant, reaching a maximum concentration of 2,364 µmol kg^{-1} in HSSW and slightly decreasing in the fresher ISW (2,353 ± 3 µmol kg^{-1}) due to the dilution effect generated by melt-water input. Both the HSSW on the shelf and the mSW on the continental slope exhibited, instead, a mean TCO_2 concentration (2,251 ± 5 and 2,255 ± 5 µmol kg^{-1}, respectively) lower than the offshore CDW source (2,259 ± 1 µmol kg^{-1}), reflecting the impact of different physical and biological processes in seasonal carbonate chemistry modification that will be discussed more in detail in *Section Influence of physical and biological processes on carbon distribution and flow*. The aragonite saturation state (Ω_{ar}, Figure 3D), computed from observations of pH_T *in situ* and TA, was generally high in surface waters, reaching supersaturate conditions (~2.3) in the biologically productive TNBp. Below the mixed layer, Ω_{ar} gradually decreased up to 1.1 value around ~800 m depth. Calcium carbonate undersaturation conditions (Ω_{ar}< 1) were observed in the deepest layers across all stations in association with minima pH_T *in situ* of ~7.998.

Biogeochemical and microbiological properties

Average vertical profiles of POC (Figure 5A) revealed surface polynya concentrations (13.9 ± 7.6 µmol kg^{-1}) significantly greater than offshore (3.8 ± 3.4 µmol kg^{-1}) and a maximum of 22.0 µmol kg^{-1} in TNBp. POC concentration declined sharply below the mixed layer of all the considered stations, becoming typically small into the deep ocean (~0.6 µmol kg^{-1}). However, in TNBp and RSp, the POC at intermediate-deep waters (0.8 ± 0.5 and 1.1 ± 0.3 µmol kg^{-1}, respectively) was considerably

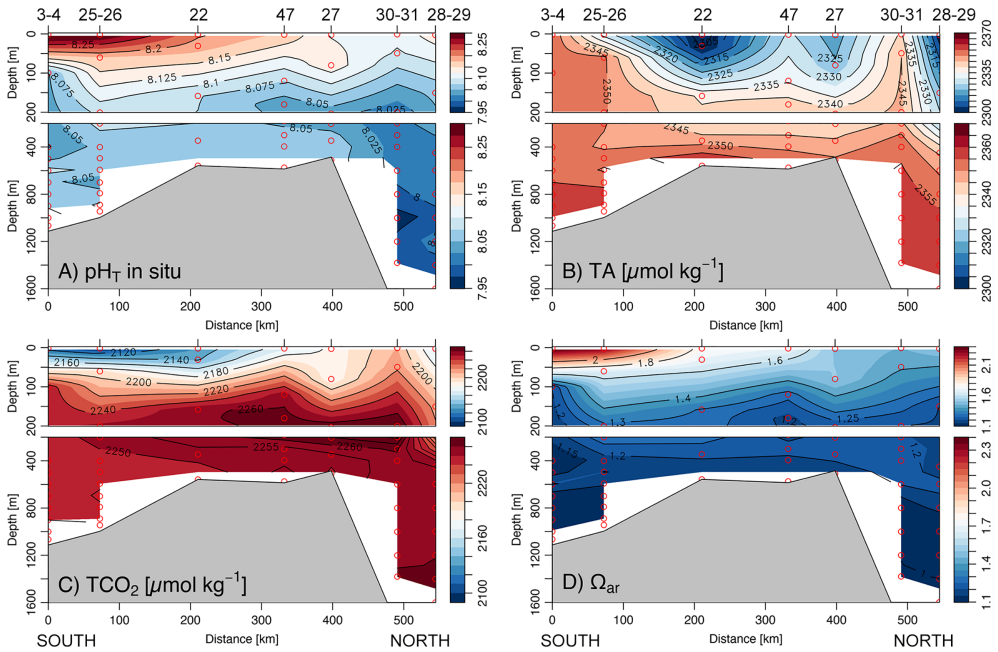

FIGURE 4
South-north vertical section across the Ross Sea (see Figure 1) for **(A)** pH_T at *in situ* temperature (pH_T *in situ*), **(B)** total alkalinity concentration (TA; µmol kg^{-1}), **(C)** dissolved inorganic carbon concentration (TCO_2; µmol kg^{-1}), and **(D)** aragonite saturation state (Ω_{ar}).

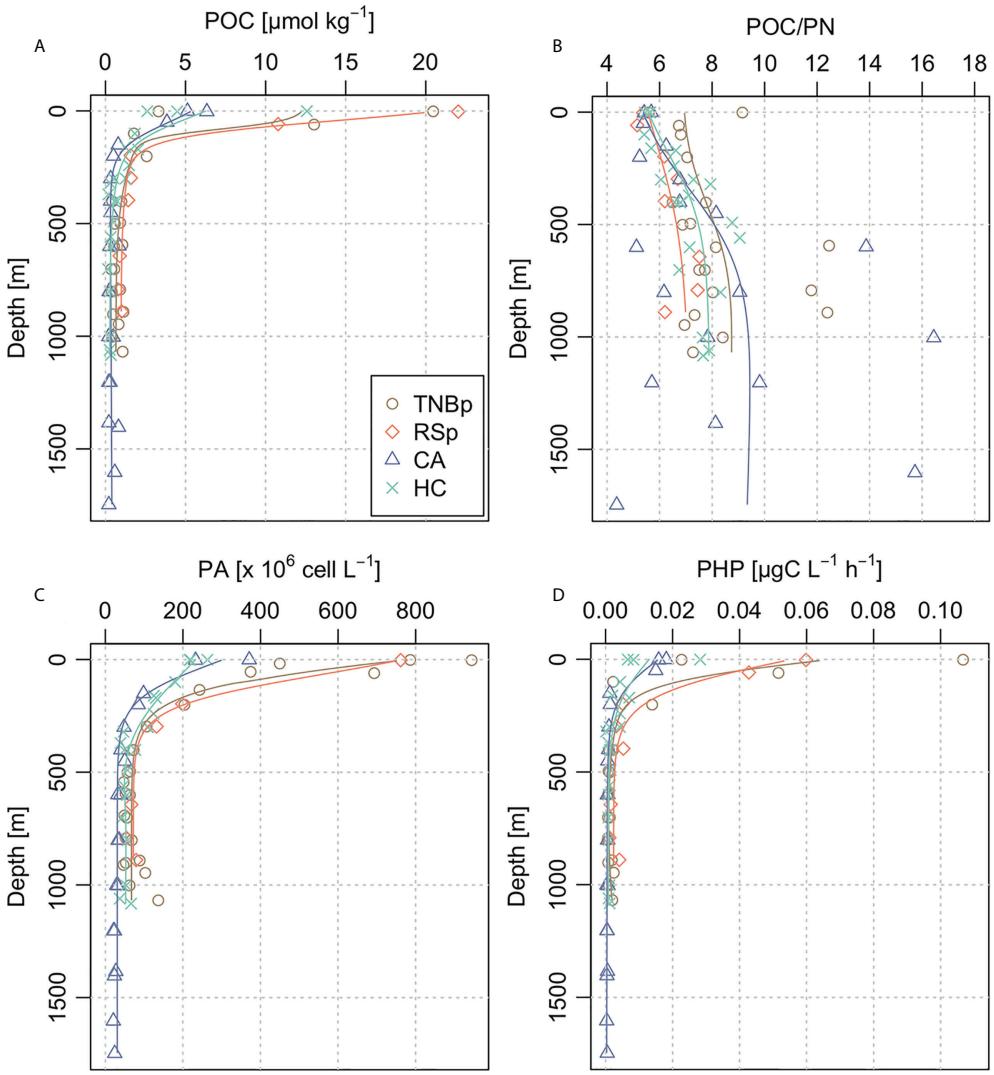

FIGURE 5
Bin-averaged profiles in the selected geographic areas of the Ross Sea (Terra Nova Bay polynya (TNBp), Ross Sea polynya (RSp), Hillary Canyon (HC), and Cape Adare (CA)) for **(A)** particulate organic carbon concentration (POC; µmol kg^{-1}), **(B)** molar ratio between particulate organic carbon and particulate nitrogen concentrations (POC/PN), **(C)** prokaryotic abundance (PA; cell L^{-1}), and **(D)** prokaryotic heterotrophic production (PHP; µgC L^{-1} h^{-1}).

higher than the measured value near the shelf break and on the continental slope (HC = 0.5 ± 0.4 µmol kg^{-1} and CA = 0.4 ± 0.2 µmol kg^{-1}), indicating important differences in the production, export, and preservation of organic carbon between shelf and offshore regions. Accordingly, the POC/PN ratio was low in the upper 200 m of the different sub-areas (6.0 ± 1.0, Figure 5B) and gradually increased with depth up to ~8.6. An anomalous sea surface ratio higher than 9 was detected in the RSp, where also a considerable increase in depth was observed. Similarly, the POC/PN profile in the offshore region of CA revealed a deep sea ratio higher and more variable than the sea surface, reaching a maximum of 16.4 at ~1,000 depth.

The PA was in the order of 10^8 cell L^{-1} in the epipelagic layer and 10^7 cell L^{-1} in the meso-bathypelagic layer, with the polynya region hosting the largest prokaryotic abundance in the upper 150 m (TNBp = 4.8 ± 3.0 × 10^8 cell L^{-1}, RSp = 7.5 ± 0.1 × 10^8 cell L^{-1}, Figure 5C). Therefore, peaks of PHP were detected at the surface of TNBp (0.10 µg C L^{-1} h^{-1}) and RSp (0.06 µg C L^{-1} h^{-1}), while the deep layers presented 2 orders of magnitude lower rates, both on the shelf and further offshore (~0.001 µg C L^{-1} h^{-1}). The overall average profile of PA and PHP (Figures 5C, D) was consistent with the vertical distribution of POC, showing a high value in the carbon-rich euphotic layer (i.e., AASW with POC = 7.0 ± 6.8 µmol kg^{-1}, PA

TABLE 2 Average concentrations of particulate organic carbon (POC; μmol kg^{-1}), the molar ratio between particulate organic carbon and particulate nitrogen (POC/PN), prokaryotic abundance (PA; cell L^{-1}), prokaryotic heterotrophic production (PHP; μgC L^{-1} h^{-1}) for each water mass in the Ross Sea.

Parameter	AASW	CDW	mCDW	mSW	HSSW	ISW	WW
POC	7.0	0.4	0.5	0.3	0.7	0.5	0.9
POC/PN	6.0	10.7	6.8	8.1	8.2	7.8	7.9
PA	38×10^7	3.3×10^7	7.1×10^7	5.2×10^7	6.9×10^7	5.3×10^7	8.6×10^7
PHP	0.0247	0.0005	0.0015	0.0011	0.0015	0.0014	0.0017

$= 3.8 \pm 2.7 \times 10^8$ cell L^{-1}, PHP = 0.02 ± 0.03 μg C L^{-1} h^{-1}) and a decreasing trend with depth. Thus, intermediate and deep waters both on the continental shelf and slope were characterized by a poor POC content and low prokaryotic activity/abundance (see Table 2).

Anthropogenic carbon and OA state

The water column distributions of C_{ant} along the South–North section are shown in Figure 6A. None of the identified water masses were old enough to be free of anthropogenic CO_2 (see Table 1). Thus, a large amount of C_{ant} was found mainly just below the mixed layer, associated with water formed on the shelf, namely mCDW (30 ± 11 μmol kg^{-1}), and ISW (31 ± 2 μmol kg^{-1}). Elevated concentration of C_{ant} was also detected in the recently ventilated WW (28 ± 3 μmol kg^{-1}) and HSSW (25 ± 3 μmol kg^{-1}), consistent with the highest concentrations of dissolved oxygen. The CDW was characterized by a very small C_{ant} accumulation (7 μmol kg^{-1}), reflecting the old ventilation time of this water mass that has long been out of contact with the atmosphere. Finally, a relatively higher C_{ant} was associated with mSW (19 ± 5 μmol kg^{-1}) due to the downslope mixing of the dense shelf waters highly enriched in C_{ant}. The estimated pH and Ω_{ar} reduction between the beginning of the Industrial Revolution (~1750) and the time of sampling (i.e., ΔpH_T and $\Delta\Omega_{ar}$) were broadly consistent with the distribution of C_{ant} (Figures 6B, C). The high C_{ant} storage in the intermediate waters of the shelf area has led to a maximum pH and Ω_{ar} decrease of −0.12 and −0.36 respectively, while offshore CDW less affected by C_{ant} revealed a lower ocean acidification impact (ΔpH_T = −0.03 ± 0.01, $\Delta\Omega_{ar}$ = −0.09 ± 0.03). The HSSW also presented significant seawater acidification from the preindustrial time (ΔpH_T = −0.07 ± 0.01, $\Delta\Omega_{ar}$ = −0.23 ± 0.03) which was further transposed along the continental slope and to the deep ocean (e.g., mSW with ΔpH_T = −0.06 ± 0.01 and $\Delta\Omega$ar = −0.18 ± 0.04). The ocean acidification found in the newly formed WW was consistent with the impact of recent anthropogenic CO_2 uptake from the atmosphere, leading to a pH and Ω_{ar} average reduction of −0.08 ± 0.01 and −0.26 ± 0.01, respectively.

Discussion

Influence of physical and biological processes on carbon distribution and flow

Studies of the CO_2 system carried out in the Ross Sea over the last decades have shown that the large seasonal variability is strongly influenced by a combination of physical and biological processes (Rivaro et al., 2014; Rivaro et al., 2017; Rivaro et al., 2019). However, the specific contributions deriving from photosynthesis/respiration, sea ice formation/melting, and air–sea CO_2 exchange remains poorly understood. Our estimate of the total integrated depletion of TCO_2 in the mixed layer (ΔTCO_2^{tot}, Figure 7A) was larger in the TNBp (−176 ± 57 mmol m^{-2}) as compared to offshore areas (e.g., −59 ± 35 mmol m^{-2} in CA). The contribution related to salinity change was dominant at all stations, accounting for more than half of the total change of TCO_2 at the polynya areas due to freshwater dilution of melting sea ice (i.e., −116 mmol m^{-2} for station 76). In polynya waters, we also observed a contribution from excess or residual TA (−26 ± 31 mmol m^{-2} in TNBp), which may either be consistent with the dissolution of abiotic calcium carbonate from the mineral ikaite ($CaCO_3{\cdot}6H_2O$) *via* the spring–summer melting sea ice, or the addition of meltwater with nonzero TA. It has been shown that ikaite crystals precipitate during sea ice formation (Rysgaard et al., 2007; Rysgaard et al., 2009; Rysgaard et al., 2012) and may remain trapped within the brine channels and pockets in the sea ice (Dieckmann et al., 2008; Dieckmann et al., 2010). During sea ice melt in spring and summer, meltwater inputs dilute TA, hence reducing the buffer capacity of the surface water. Accordingly, ikaite is released back to the surface water and may dissolve, leading to an enrichment of TA relative to TCO_2 (Hauri et al., 2015; Legge et al., 2017; Jones et al., 2017; Jones et al., 2021). Our observations confirm this process to be relevant in the TNBp area; however, improved characterization of the TA (and TCO_2) in sea ice is needed to more accurately assess the potential contribution of meltwater with residual TA to the overall seasonal TCO_2 change.

The polynya waters were also distinct in terms of enhanced biological CO_2 drawdown (e.g., −90 ± 26 mmol m^{-2} in the TNBp,

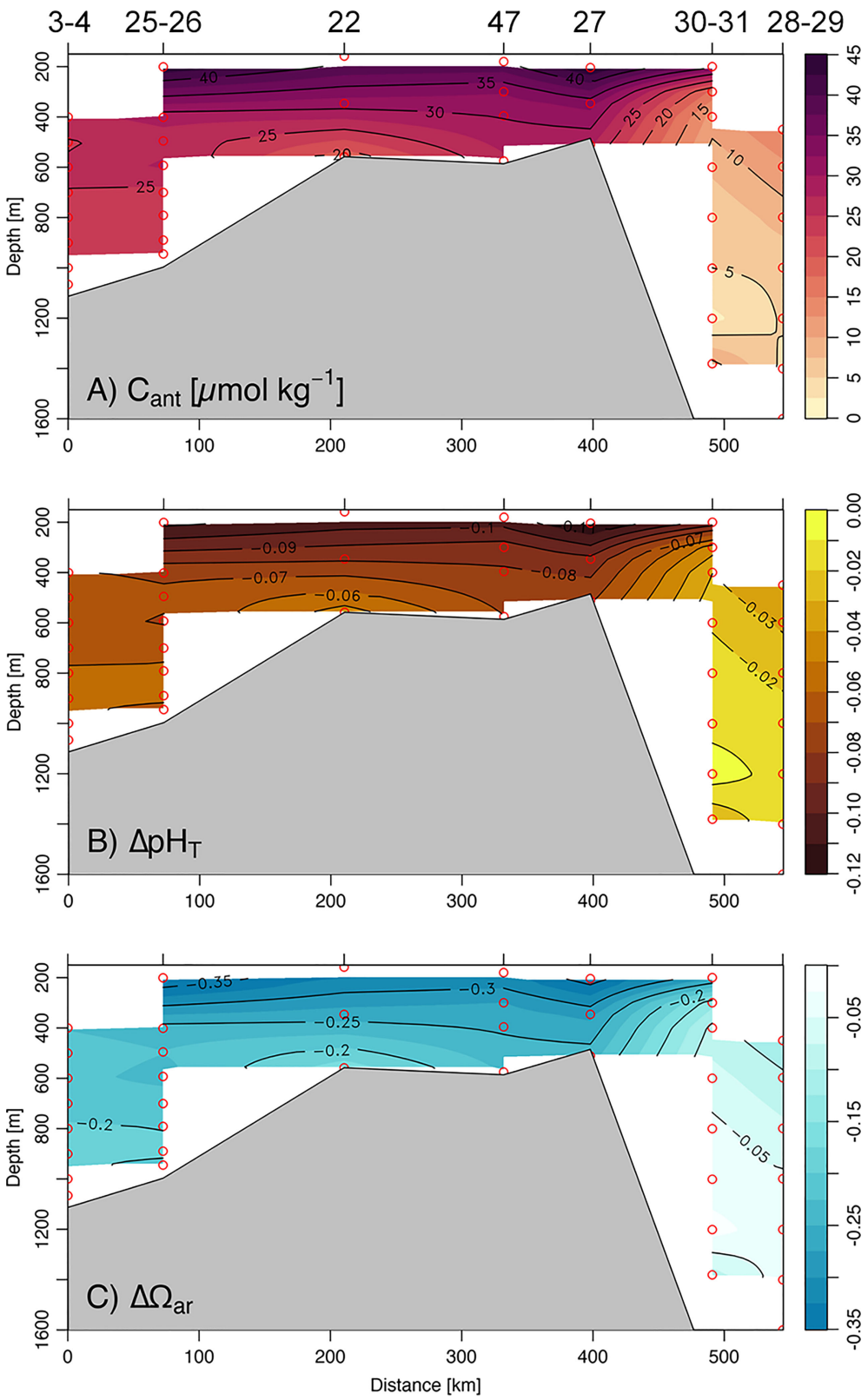

FIGURE 6
South-north vertical section across the Ross Sea (see Figure 1) for **(A)** anthropogenic carbon concentration (C_{ant}; µmol kg^{-1}), **(B)** pH reduction from preindustrial time (ΔpH_T), and **(C)** aragonite reduction from preindustrial time ($\Delta\Omega_{ar}$).

Figure 7A), consistent with the average estimation of NCP (−136 ± 52 mmol m^{-2} day^{-1} Figure 7B) and suggesting a strong autotrophic condition of the coastal zone. Our NCP results are in good agreement with previous studies from the Ross Sea that estimated early summer primary productivity based on different methods. For example, Smith and Gordon (1997) found a depth integrated primary production of −127 ± 61 mmol m^{-2} day^{-1} by using the ^{14}C -incubation technique. Similarly, Arrigo et al. (2000) estimated a ^{14}C PP of −111 mmol m^{-2} day^{-1}, which was consistent with a satellite-based primary productivity estimate (−104 mmol m^{-2} day^{-1}) and NCP determined from the seasonal reduction of TCO_2 (−107 mmol m^{-2} day^{-1}) and nitrate (−95 mmol m^{-2} day^{-1}). In the offshore waters, NCP gradually decreased to roughly −80 mmol m^{-2} day^{-1}, even though the dominance of primary production over respiration persisted, and this confirmed the net biological CO_2 drawdown as a widespread condition of the Ross Sea during summer.

The Ross Sea has been extensively recognized as the most productive region of the Southern Ocean, with an annual primary production rate of approximately 83.4 Tg C $year^{-1}$ (Smith and Gordon, 1997; Smith et al., 2006; Arrigo et al., 2008b; Catalano et al., 2010). In the TNBp, DeJong et al. (2017) observed an extraordinary summer NCP of −425 ± 204 mmol m^{-2} day^{-1}, which represented the highest biological production yet reported from the Ross Sea and was an order of magnitude larger than any other Antarctic coastal polynya (e.g., NCP in Dalton Polynya ranging from −10 to −20 mmol m^{-2} day^{-1}, Arroyo et al., 2019; in Mertz Polynya ranging from −11 to −78 mmol m^{-2} day^{-1}, Sambrotto et al., 2003; Shadwick et al., 2014; Shadwick et al., 2017; in Prydz Bay with an average of −15 ± 3 mmol m^{-2} day^{-1}, Roden et al., 2013). The NCP estimated in our study confirms the Ross Sea coastal area to be a major site for biological production and associated TCO_2 reduction in the surface mixed layer. However, with respect to the huge NCP of DeJong et al. (2017) observed in late summer (12 February to 18 March 2013), our NCP rate was estimated during early summer (11 January to 4 February 2014) and presented a slightly lower mean value. This probably reflects an intrinsic variability in the timing of production, seasonal progression of phytoplankton assemblages, mesoscale variations, and influences of different physical constraints. During spring–early summer, biological production occurs in a mixed layer of approximately 50 m deep, and phytoplankton communities are generally dominated by *Phaeocystis antarctica* (Smith and Gordon, 1997; Arrigo et al., 1999), due to its ability to photosynthesize under reduced irradiances (Kropuenske et al., 2009). As the summer season moves on, a more intense biological production is sustained by diatoms and a shallower mixed layer (~10 m) concentrate algal biomass towards the surface. As described by DeJong et al. (2017), a final enhanced late season NCP could be driven by strong katabatic winds (up to 27 ms^{-1}) that may resupply nutrients/trace elements (e.g., iron) from the depths and generate ideal conditions for Langmuir circulation cells and exceptional early formation of new frazil ice crystals, both concentrating diatoms into discrete rows at the sea surface where the light can boost productivity.

The observed highest NCP in the polynya area (TNBp and RSp) was associated with a large summer surplus of POC (12.6 ± 10.1 mmol m^{-2} day^{-1}, Figure 7C) and intense prokaryotic activity (95.9 ± 60.6 mg C m^{-2} day^{-1}, Figure 7D), while offshore stations (CA and HC area) presented significantly lower values. An analysis of late summer carbon export by DeJong et al. (2017) revealed that about 70% of the carbon fixed into biomass by primary producers in the Ross Sea surface layer is quickly exported as POC below 200 m depth, where organic carbon is then remineralized back to CO_2 by microbial respiration. According to sediment-trap estimates, the degradation of organic carbon that sinks to the Ross Sea interior may represent up to 67% of the total POC flux (Azzaro et al., 2006; Chiarini et al., 2019), yet it has been proven that different particle-associated-prokaryotic communities with specific exoenzymatic activities are responsible for high remineralization rates (Manna et al., 2020). Such a mechanism is consistent with our estimates of large ΔPOC and associated PHP in polynya waters, which may explain the observed high concentration of anthropogenic CO_2 at the top of the mesopelagic zone (~200–300 m, Figure 6A). Organic particles may indeed be subjected to fast remineralization, leading to the release of previously overlooked anthropogenic CO_2 and contributing to the ocean acidification of the intermediate layer of the Ross Sea (Figure 6C). It is worth noting that an undefined amount of anthropogenic CO_2 could also derive from the microbial degradation of the dissolved organic carbon (DOC), which represents a relevant component of the organic carbon pool of the Ross Sea. However, previous studies on the remineralization in the euphotic zone of the Ross Sea highlighted a very low flux of carbon through the DOC (Celussi et al., 2009), and Bercovici et al. (2017) reported a DOC enrichment (~7 μmol kg^{-1}) in dense shelf waters. These findings suggest that microbial degradation of DOC could contribute only slightly to the high concentration of anthropogenic CO_2 in the upper mesopelagic zone observed in our study. The sequestration of refractory DOC into the deep ocean may represent a hidden pathway of anthropogenic CO_2 sink which has never been quantified and warrants further investigation.

Anthropogenic carbon storage and export

The combination of high primary production, rapid carbon export below the upper mixed layer, and strong katabatic winds in the Ross Sea results in a large undersaturation of surface pCO_2 and extremely high atmospheric CO_2 uptake. In TNBp, DeJong and Dunbar (2017) reported a CO_2 flux from the atmosphere to the sea surface of −72 ± 32 mmol m^{-2} day^{-1}, with an extraordinary instantaneous flux of up to −246 mmol m^{-2}

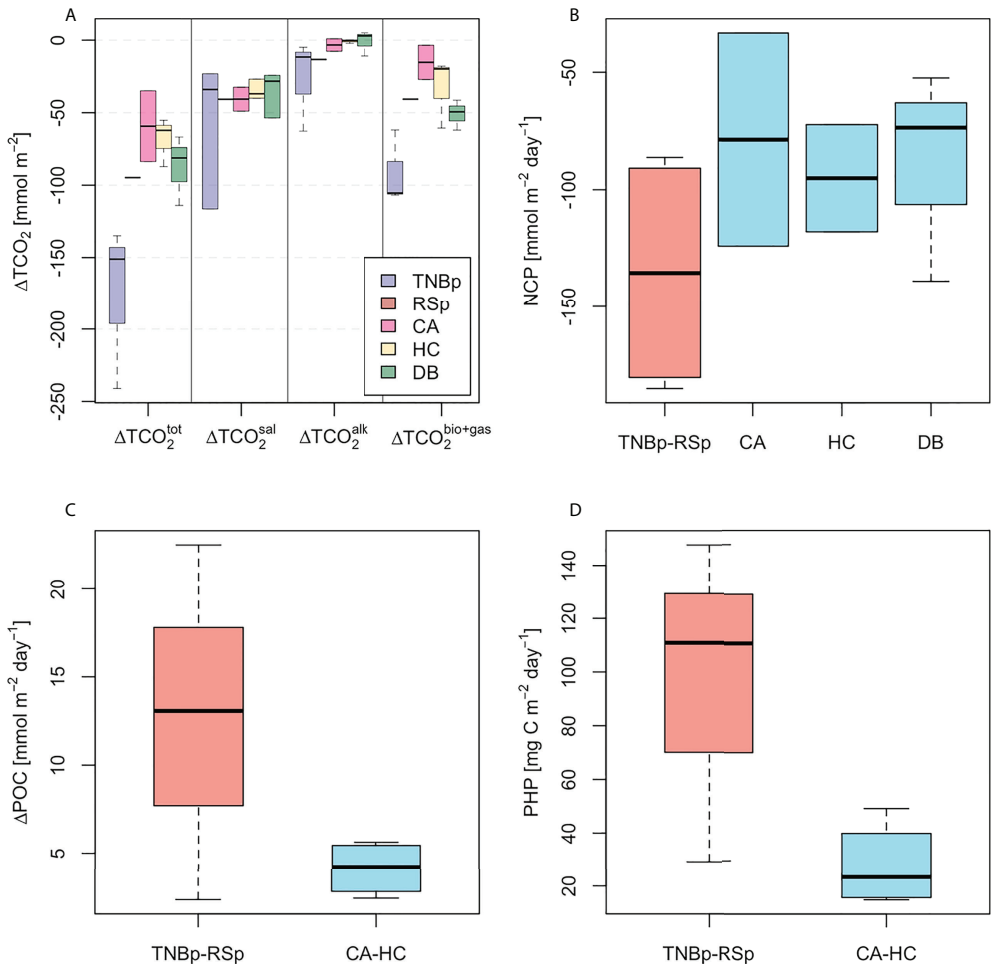

FIGURE 7
(A) Total deficit of TCO_2 (ΔTCO_2^{tot}; mmol m^{-2}) in the mixed-layer for each region and contribution from salinity (ΔTCO_2^{sal}, mmol m^{-2}), carbonate mineral processes (ΔTCO_2^{alk}, mmol m^{-2}), biology, and gas exchange ($\Delta TCO_2^{bio-gas}$, mmol m^{-2}). **(B)** Mean net community production (NCP, mmol m^{-2} day^{-1}), **(C)** surplus of particulate organic carbon (ΔPOC, mmol m^{-2} day^{-1}), and **(D)** prokaryotic heterotrophic production (PHP; mg C m^{-2} day^{-1}) in the 0–200–m layer for each region.

day^{-1}, which is stronger than any other Antarctic coastal zone, such as Amundsen Polynya (−36 ± 8.4 mmol m^{-2} day^{-1}; Mu et al., 2014), Mertz Polynya (−15 mmol m^{-2} day^{-1}; Shadwick et al., 2014), and Gerlache Strait (−31 ± 19 mmol m^{-2} day^{-1}, Monteiro et al., 2020). In addition, the estimated atmospheric CO_2 uptake in TNBp was three to four times more intense than that in the open waters of the Ross Sea (on the order of −15 mmol m^{-2} day^{-1}, Monteiro et al., 2020), where net air–sea CO_2 flux is driven by a lower biological production and large mesoscale variability of surface pCO_2 (Rivaro et al., 2017; Rivaro et al., 2019). Overall, such estimates of air–sea CO_2 fluxes confirm that the anthropogenic CO_2 sink is likely to be very intense in the Ross Sea. Chen (1994) reported a CO_2 excess of 25 ± 10 µmol kg^{-1} in the HSSW around Cape Adare, while Sandrini et al. (2007) estimated a C_{ant} concentration of 30 ± 4 µmol kg^{-1} in the ventilated shelf waters of the Ross Sea by using the TrOCA method based upon measurements carried out in summer 2003. Furthermore, in the Ross Sea shelf waters, Arrigo et al. (2008a) with a coupled physical/biogeochemical model calculated a C_{ant} concentration of approximately 12–25 µmol kg^{-1} throughout the water column, in good agreement with recent estimates by Pardo et al. (2014) for different water masses of the Southern Ocean, obtained also by the TrOCA method, who found a C_{ant} content of 25.0 ± 4 µmol kg^{-1} for the layer comprising both HSSW and AASW.

Thus, the average C_{ant} value reported here for dense shelf waters, namely HSSW (25 ± 3 µmol kg^{-1}), ISW (31 ± 2 µmol kg^{-1}), WW (28 ± 3 µmol kg^{-1}), are within the range expected considering previous estimates carried out in the Ross Sea, and it is consistent with the value detected in other regions of AABW

formation. In Cape Darnley, Roden et al. (2016) observed high C_{ant} concentrations (25 ± 3 µmol kg^{-1}) in the bottom water, deriving from water masses over the shelf heavily enriched in C_{ant} (53 ± 3 µmol kg^{-1}). Anderson et al. (1991) measured the C_{ant} in the Southern Weddell Sea continental shelf and reported a C_{ant} concentration of 36 µmol kg^{-1} in the ISW. Finally, Kerr et al. (2018) and Shadwick et al. (2014) estimated, throughout the TrOCA method, an average C_{ant} content of 30 ± 6 and 40–44 µmol kg^{-1} in the dense shelf water of the Gerlache Strait and Mertz polynya region, respectively.

In our study, the largest C_{ant} concentration (38 ± 6 µmol kg^{-1}) was observed, however, directly below the mixed layer, associated with the mCDW between roughly 120 and 300 m. This water mass, sourced by the interaction of inflowing C_{ant}-poor CDW with AASW, presented peculiar biogeochemical properties that can reveal the contribution of biological processes to the overall anthropogenic CO_2 sequestration capacity of the Ross Sea. The transition from AASW to mCDW was associated with a utilization of 83 µmol kg^{-1} of DO and an accumulation of 70 µmol kg^{-1} of TCO_2 (salinity-normalized). According to the Redfield ratio of CO_2: O_2 = 106: 138 for organic matter remineralization, we would expect, from the observed O_2 utilization, an increase of ~64 of respiratory TCO_2. This value is very close to the estimated TCO_2 change from AASW to mCDW, indicating a contribution from remineralization that is much greater than the CO_2 uptake from the atmosphere.

Therefore, different physical and biological processes influence the anthropogenic CO_2 sink of the Ross Sea, which can be described following its oceanographic properties (Figure 8). Summer biological production modifies the surface waters on the shelf by reducing the TCO_2 and enhances the photosynthetic fixation of anthropogenic carbon into particulate organic matter. This biomass is subsequently transferred below the mixed layer where the biologically overlocked anthropogenic carbon is remineralized back to CO_2 and, through mixing with C_{ant}-poor CDW intruding from offshore, increases the C_{ant} concentration of mCDW beyond the levels that could be determined by air–sea CO_2 exchange alone (Figure 8). The onset of the winter season and associated dense water formation represent a pathway for anthropogenic carbon transfer from the atmosphere into the deep ocean. In the polynya system, sea-ice production drives deep convection due to brine rejection, and surface waters may become supersaturated due to both mixing with TCO_2-rich subsurface water and the uptake of considerable amounts of atmospheric CO_2, likely enhancing the C_{ant} concentration in dense shelf waters (Figure 8). Finally, the outflow of water across the slope is a mixture of dense shelf waters with CDW (i.e., mSW), which sequesters a large quantity of anthropogenic carbon into the ocean interior for hundreds of years (England, 1995).

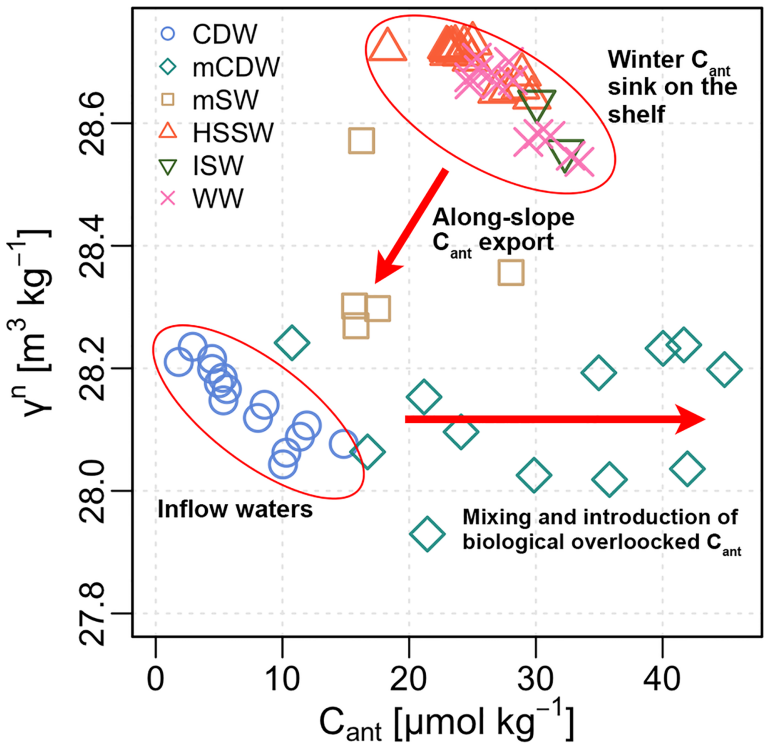

FIGURE 8
Neutral density anomaly (γ^n; kg, m^{-3}) vs. C_{ant} (µmol kg^{-1}) concentrations for each identified water mass, along with oceanographic and biogeochemical processes driving the observed C_{ant} distribution in the Ross Sea.

How the anthropogenic carbon sink capacity of the Ross Sea will respond to climate change remains uncertain. With the reduction of sea ice extent, increased areas of open waters could enhance the anthropogenic CO_2 transfer across the ocean-atmosphere interface (Loose et al., 2014) and increase the strength of the biological carbon pump (Bernardello et al., 2014; Ito et al., 2015). At the same time, however, ocean warming reduces the solubility of CO_2 and is projected to decrease the oceanic CO_2 uptake by ~10% (Plattner et al., 2001). Model studies have also predicted that the ocean's overturning circulation will weaken as the ocean becomes warmer and more stratified. This will drastically reduce the deep convection in high latitude regions and less C_{ant} will be sequestered into the deep ocean (Matear and Hirst, 1999; Bernardello et al., 2014; Holzer et al., 2020). It is not clear which of these opposing effects will be more important, and therefore high-resolution observations and models are needed to provide a better understanding of the future anthropogenic CO_2 sink of the Ross Sea.

Conclusions

This work provides new insights into the physical and biological controls of anthropogenic CO_2 sinks of the Ross Sea during the summer season through the integration of carbonate system observations with biogeochemical properties of the water masses. The polynya surface waters showed relatively high seasonal TCO_2 reduction, mainly driven by freshwater dilution of melting sea ice. Intense biological production was also found here, leading to enhanced uptake of anthropogenic CO_2 into particulate organic matter. The observations showed that a large amount of this biomass was quickly mobilized back to CO_2 by microbial respiration, revealing a significant contribution of the "microbial shunt of anthropogenic carbon" to the upper mesopelagic zone. How this process could affect the biological carbon pump efficiency is currently unknown; however, we found that a combination of high NCP and rapid carbon export below the mixed layer caused surface CO_2 to remain broadly below the saturation level, preconditioning the winter for a large C_{ant} uptake into dense shelf waters. Overall, this resulted in a significant ocean acidification of the Ross Sea, which already leads to calcium carbonate undersaturation conditions of the deepest ocean layers with a critical impact on calcifying organisms. Improved understanding of anthropogenic carbon dynamics and sink capacity of the coastal Southern Ocean to future environmental changes (i.e., increased atmospheric CO_2, rising temperatures, sea-ice reduction, ocean circulation change, and modification of biological CO_2 drawdown) will require intensified long-term observations of the carbonate system and ocean biogeochemistry to be combined into holistic models.

Data availability statement

The datasets presented in this study can be found in online repositories. The names of the repository/repositories and accession number(s) can be found below: OGS National Oceanographic Data Center (NODC) https://nodc.ogs.it/catalogs/doidetails?3&doi=10.13120/cfeaa3ca-2b9c-445f-be27-a74e346026ba.

Author contributions

GI, MG, and MC conceptualized the study. MC acquired the funding and managed the project. LZ and MC collected samples. GB and PC elaborated physical oceanography data. GI elaborated chemical data with the support of MG and PR. GI, MK, CC, LZ, and MC performed the laboratory analyses. GI wrote the manuscript with the help and input from all co-authors. All authors contributed to the article and approved the submitted version.

Funding

This study was supported by the project DEEPROSSS (DEEP ROSS Sea ecosystem functioning: new insights on the role of ventilation on microbial metabolism and diversity) in the framework of the Italian Program for Research in Antarctica (project PNRA 2013/AN1.01) with funds from the Italian Ministry of Education, University and Research (MIUR). The contribution by GI was supported by the "Centro Aldo Pontremoli," part of the ENI-CNR Joint Research Agreement.

Acknowledgments

The authors are grateful to G. De Carolis (CNR), R. Geletti (OGS), the crew of the R/V Italica, and the team from ENEA for their help during sampling. Dan Kelley and Clark Richards are kindly acknowledged for their help in the use of the "OCE" package. We thank the reviewers and the editor, whose constructive comments improved the overall quality of the manuscript.

Conflict of interest

The authors declare that the research was conducted in the absence of any commercial or financial relationships that could be construed as a potential conflict of interest.

Publisher's note

References

Álvarez, M., Lo Monaco, C., Tanhua, T., Yool, A., Oschlies, A., Bullister, J. L., et al. (2009). Estimating the storage of anthropogenic carbon in the subtropical Indian Ocean: A comparison of five different approaches. *Biogeosciences* 6, 681–703. doi: 10.5194/bg-6-681-2009

Anderson, L. G., Holby, O., Lindegren, R., and Ohlson, M. (1991). The transport of anthropogenic carbon dioxide into the Weddell Sea. *J. Geophys. Res.: Oceans* 96 (C9), 16679–16687. doi: 10.1029/91JC01785

Arndt, J. E., Schenke, H. W., Jakobsson, M., Nitsche, F., Buys, G., Goleby, B., et al. (2013). The international bathymetric chart of the Southern Ocean (IBCSO) version 1.0 - a new bathymetric compilation covering circum-antarctic waters. *Geophys. Res. Lett.* 40, 3111–3117. doi: 10.1002/grl.50413

Arrigo, K. R., DiTullio, G. R., Dunbar, R. B., Robinson, D. H., VanWoert, M., Worthen, D. L., et al. (2000). Phytoplankton taxonomic variability in nutrient utilization and primary production in the Ross Sea. *J. Geophys. Res.: Oceans* 105 (C4), 8827–8846. doi: 10.1029/1998JC000289

Arrigo, K. R., and McClain, C. R. (1994). Spring phytoplankton production in the Western Ross Sea. *Science* 266 (5183), 261–263. doi: 10.1126/science.266.5183.261

Arrigo, K. R., Robinson, D. H., Worthen, D. L., Dunbar, R. B., DiTullio, G. R., VanWoert, M., et al. (1999). Phytoplankton community structure and the drawdown of nutrients and CO_2 in the Southern Ocean. *Science* 283 (5400), 365–367. doi: 10.1126/science.283.5400.365

Arrigo, K. R., and van Dijken, G. L. (2004). Annual changes in sea-ice, chlorophyll a, and primary production in the Ross Sea, Antarctica. *Deep Sea Res. Part II: Topical Stud. Oceanogr.* 51 (1-3), 117–138. doi: 10.1016/j.dsr2.2003.04.003

Arrigo, K. R., van Dijken, G. L., and Bushinsky, S. (2008b). Primary production in the Southern Ocean 1997–2006. *J. Geophys. Res.* 113, C08004. doi: 10.1029/2007JC004551

Arrigo, K. R., van Dijken, G. L., and Long, M. (2008a). Coastal Southern Ocean: A strong anthropogenic CO_2 sink, geophys. *Res. Lett.* 35, L21602. doi: 10.1029/2008GL035624

Arrigo, K. R., van Dijken, G. L., and Strong, A. L. (2015). Environmental controls of marine productivity hot spots around Antarctica. *J. Geophys. Res.: Oceans* 120 (8), 5545–5565. doi: 10.1002/2015JC010888

Arroyo, M. C., Shadwick, E. H., and Tilbrook, B. (2019). Summer carbonate chemistry in the Dalton Polynya, East Antarctica.. *J. Geophys. Res. Oceans* 124, 5634–5653. doi: 10.1029/2018JC014882

Arroyo, M. C., Shadwick, E. H., Tilbrook, B., Rintoul, S. R., and Kusahara, K. (2020). A continental shelf pump for CO_2 on the Adélie Land coast, East Antarctica. *J. Geophys. Res. Oceans* 125, 59–22. doi: 10.1029/2020JC016302

Azouzi, L., Goyet, C., Goncalves, R. I., and Touratier, F. (2009). Anthropogenic carbon distribution in the eastern South Pacific Ocean. *Biogeosciences* 6, 149–156. doi: 10.5194/bg-6-149-2009

Azzaro, M., La Ferla, R., and Azzaro, F. (2006). Microbial respiration in the aphotic zone of the Ross Sea (Antarctica). *Mar. Chem.* 99 (1-4), 199–209. doi: 10.1016/j.marchem.2005.09.011

Bates, N. R., Hansell, D. A., Carlson, C. A., and Gordon, L. I. (1998). Distribution of CO_2 species, estimates of net community production, and air-sea CO_2 exchange in the Ross Sea polynya. *J. Geophys. Res.* 103 (C2), 2883–2896. doi: 10.1029/97jc02473

Bates, N. R., and Johnson, R. J. (2020). Acceleration of ocean warming, salinification, deoxygenation and acidification in the surface subtropical North Atlantic Ocean. *Commun. Earth Environ.* 1 (1), 1–12. doi: 10.1038/s43247-020-00030-5

Bercovici, S. K., Huber, B. A., DeJong, H. B., Dunbar, R. B., and Hansell, D. A. (2017). Dissolved organic carbon in the Ross Sea: Deep enrichment and export. *Limnol. Oceanogr.* 62 (6), 2593–2603. doi: 10.1002/lno.10592

Bernardello, R., Marinov, I., Palter, J. B., Galbraith, E. D., and Sarmiento, J. L. (2014). Impact of Weddell Sea deep convection on natural and anthropogenic carbon in a climate model. *Geophys. Res. Lett.* 41 (20), 7262–7269. doi: 10.1002/2014GL061313

Brewer, P. G., and Goldman, J. C. (1976). Alkalinity changes generated by phytoplankton growth. *Limnol. Oceanogr.* 21 (1), 108–117. doi: 10.4319/lo.1976.21.1.0108

Budillon, G., Castagno, P., Aliani, S., Spezie, G., and Padman, L. (2011). Thermohaline variability and antarctic bottom water formation at the Ross Sea shelf break. *Deep Sea Res. I Oceanogr. Res. Pap.* 58 (10), 1002–1018. doi: 10.1016/j.dsr.2011.07.002

Budillon, G., Pacciaroni, M., Cozzi, S., Rivaro, P., Catalano, G., Ianni, C., et al. (2003). An optimum multiparameter mixing analysis of the shelf waters in the Ross Sea. *Antarct. Sci.* 15, 105–118. doi: 10.1017/S095410200300110X

Carvalho, F., Kohut, J., Oliver, M. J., and Schofield, O. (2017). Defining the ecologically relevant mixed-layer depth for Antarctica's coastal seas. *Geophys. Res. Lett.* 44, 338–345. doi: 10.1002/2016GL071205

Castagno, P., Falco, P., Dinniman, M. S., Spezie, G., and Budillon, G. (2017). Temporal variability of the circumpolar deep water inflow onto the Ross Sea continental shelf. *J. Mar. Syst.* 166, 37–49. doi: 10.1016/j.jmarsys.2016.05.006

Catalano, G., Budillon, G., La Ferla, R., Povero, P., Ravaioli, M., Saggiomo, V., et al. (2010). "The Ross Sea," in *Carbon and nutrient fluxes in continental margins: A global synthesis*. Eds. L. Liu, K.-K. Atkinson, L. Quinones and R. Talaue-McManus (Berlin: Springer), 303–317.

Celussi, M., Cataletto, B., Umani, S. F., and Del Negro, P. (2009). Depth profiles of bacterioplankton assemblages and their activities in the Ross Sea. *Deep Sea Res. Part I: Oceanogr. Res. Pap.* 56 (12), 2193–2205. doi: 10.1016/j.dsr.2009.09.001

Chen, C. T. A. (1994). Some indications of excess CO_2 penetration near cape adare off the Ross Sea. *La mer* 32, 167–172.

Chiarini, F., Ravaioli, M., and Capotondi, L. (2019). Interannual variability of vertical particle fluxes in the Ross Sea (Antarctica). *Nat. Conserv.* 34, 417–440. doi: 10.3897/natureconservation.34.30732

Coale, K. H., Gordon, R. M., and Wang, X. (2005). The distribution and behavior of dissolved and particulate iron and zinc in the Ross Sea and antarctic circumpolar current along 170 w. *Deep Sea Res. Part I: Oceanogr. Res. Pap.* 52 (2), 295–318. doi: 10.1016/j.dsr.2004.09.008

de Carvalho-Borges, M., Orselli, I. B. M., de Carvalho Ferreira, M. L., and Kerr, R. (2018). Seawater acidification and anthropogenic carbon distribution on the continental shelf and slope of the western South Atlantic Ocean. *J. Mar. Syst.* 187, 62–81. doi: 10.1016/j.jmarsys.2018.06.008

DeJong, H. B., and Dunbar, R. B. (2017). Air-sea CO_2 exchange in the Ross Sea, Antarctica. *J. Geophys. Res.-Ocean* 122, 8167–8181. doi: 10.1002/2017JC012853

DeJong, H. B., Dunbar, R. B., Koweek, D. A., Mucciarone, D. A., Bercovici, S. K., and Hansell, D. A. (2017). Net community production and carbon export during the late summer in the Ross Sea, Antarctica. *Global Biogeochem. Cycles* 31 (3), 473–491. doi: 10.1002/2016GB005417

Dickson, A. G. (1990). Standard potential of the reaction – AgCl(S) +1/2h-2(G) = Ag(S) + HCl(Aq) and the standard acidity constant of the ion HSO4- in synthetic sea water from 273.15 to 318.15 k. *J. Chem. Thermodyn.* 22, 113–127. doi: 10.1016/0021-9614(90)90074-Z

Dickson, A. G., Sabine, C. L., and Christian, J. R. (2007). Guide to best practices for ocean CO_2 measurements. *PICES Spec. Publ.* 3, 191.

Dieckmann, G. S., Nehrke, G., Papadimitriou, S., Gottlicher, J., Steininger, R., Kennedy, H., et al. (2008). Calcium carbonate as ikaite crystals in antarctic sea ice, geophys. *Res. Lett.* 35, L08501. doi: 10.1029/2008GL033540

Dieckmann, G. S., Nehrke, G., Uhlig, C., Göttlicher, J., Gerland, S., Granskog, M. A., et al. (2010). Brief communication: Ikaite ($CaCO_3 \bullet 6H_2O$) discovered in Arctic sea ice. *Cryosphere* 4 (2), 227–230. doi: 10.5194/tc-4-227-2010

England, M. H. (1995). The age of water and ventilation timescales in a global ocean model. *J. Phys. Oceanogr.* 25 (11), 2756–2777. doi: 10.1175/1520-0485(1995)025<2756:TAOWAV>2.0.CO;2

Fetterer, F., Knowles, K., Meier, W. N., Savoie, M., and Windnagel, A. K. (2017). "Updated daily. sea ice index, version 3," in *Monthly and daily GIS compatible shapefiles of median ice extent* (Boulder, Colorado USA: NSIDC: National Snow and Ice Data Center). doi: 10.7265/N5K072F8

Fitzwater, S. E., Johnson, K. S., Gordon, R. M., Coale, K. H., and Smith, W. O.Jr. (2000). Trace metal concentrations in the Ross Sea and their relationship with nutrients and phytoplankton growth. *Deep Sea Res. Part II: Topical Stud. Oceanogr.* 47 (15-16), 3159–3179. doi: 10.1016/S0967-0645(00)00063-1

Gattuso, J.-P., Epitalon, J.-M., and Lavigne, H. (2015). *Seacarb: Seawater carbonate chemistry* (R Package Version 3.0.14). Available at: https://cran.rproject.org/web/packages/seacarb/index.html.

Gordon, A. L., Huber, B. A., and Busecke, J. (2015). Bottom water export from the Western Ross Sea 2007 through 2010. *Geophys. Res. Lett.* 42 (13), 5387–5394. doi: 10.1002/2015GL064457

Goyet, C., Ito, R. G., and Touratier, F. (2009). Anthropogenic carbon distribution in the eastern South Pacific Ocean. *Biogeosciences* 6, 149–156. doi: 10.5194/bg-6-149-2009

Grasshoff, K. (1983). "Determination of oxygen," in *Methods of seawater analysis*. Eds. K. Grasshoff, M. Ehrhardt and K. Kremling (WeinheimVerlag Chemie), 61–72.

Gruber, N., Gloor, M., Fletcher, S. E. M., Doney, S. C., Dutkiewicz, S., Follows, M. J., et al. (2009). Oceanic sources, sinks, and transport of atmospheric CO_2. *Global Biogeochem. Cy* 23, GB1005. doi: 10.1029/2008GB003349

Gruber, N., Landschützer, P., and Lovenduski, N. S. (2019). The variable Southern Ocean carbon sink. *Annu. Rev. Mar. Sci.* 11, 159–186. doi: 10.1146/annurev-marine-121916-063407

Hansen, H. P., and Koroleff, F. (1999). "Determination of nutrients," in *Methods of seawater analysis*, *3rd edn*. Eds. K. Grasshoff, K. Kremling and M. Ehrhardt (Weinheim: Wiley-VCH), 159–228.

Hassoun, A. E. R., Gemayel, E., Krasakopoulou, E., Goyet, C., Saab, M. A. A., Guglielmi, V., et al. (2015). Acidification of the Mediterranean Sea from anthropogenic carbon penetration. *Deep Sea Res. Part I: Oceanogr. Res. Pap.* 102, 1–15. doi: 10.1016/j.dsr.2015.04.005

Hauri, C., Doney, S. C., Takahashi, T., Erickson, M., Jiang, G., and Ducklow, H. W. (2015). Two decades of inorganic carbon dynamics along the West Antarctic Peninsula. *Biogeosciences* 12 (22), 6761–6779. doi: 10.5194/bg-12-6761-2015

Holzer, M., Chamberlain, M. A., and Matear, R. J. (2020). Climate-driven changes in the ocean's ventilation pathways and time scales diagnosed from transport matrices. *J. Geophys. Res.: Oceans* 125 (10), e2020JC016414. doi: 10.1029/2020JC016414

Huertas, I. E., Ríos, A. F., García-Lafuente, J., Makaoui, A., Rodríguez-Gálvez, S., Sánchez- Román, F. F., et al. (2009). Anthropogenic and natural CO_2 exchange through the Strait of Gibraltar. *Biogeosciences* 6, 647–662. doi: 10.5194/bg-6-647-2009

Ingrosso, G., Bensi, M., Cardin, V., and Giani, M. (2017). Anthropogenic CO_2 in a dense water formation area of the Mediterranean Sea. *Deep-Sea Res. Part I* 123, 118–128. doi: 10.1016/j.dsr.2017.04.004

Ito, T., Bracco, A., Deutsch, C., Frenzel, H., Long, M., and Takano, Y. (2015). Sustained growth of the Southern Ocean carbon storage in a warming climate. *Geophys. Res. Lett.* 42 (11), 4516–4522. doi: 10.1002/2015GL064320

Jacobs, S. S., Amos, A. F., and Bruchhausen, P. M. (1970). Ross Sea oceanography and antarctic bottom water formation. *Deep Sea Res. Oceanogr. Abstr* 17 (6), 935–962. doi: 10.1016/0011-7471(70)90046-X

Jones, E., Bakker, D., Venables, H., Whitehouse, M., Korb, R., and Watson, A. (2010). Rapid changes in surface water carbonate chemistry during antarctic sea ice melt. *Tellus B: Chem. Phys. Meteorol.* 62 (5), 621–635. doi: 10.1111/j.1600-0889.2010.00496.x

Jones, E. M., Fenton, M., Meredith, M. P., Clargo, N. M., Ossebaar, S., Ducklow, H. W., et al. (2017). Ocean acidification and calcium carbonate saturation states in the coastal zone of the West Antarctic Peninsula. *Deep Sea Res. Part II: Topical Stud. Oceanogr.* 139, 181–194. doi: 10.1016/j.dsr2.2017.01.007

Jones, E. M., Hoppema, M., and Bakker, K. (2021). Calcium carbonate saturation states along the West Antarctic Peninsula. *Antarctic Sci* 33 (6), 575–595. doi: 10.1017/S0954102021000456&domain=pdf

Kelley, D. E. (2018). "The OCE package," in *Oceanographic analysis with r* (New York, NY: Springer), 91–101.

Kerr, R., Goyet, C., da Cunha, L. C., Orselli, I. B. M., Lencina- Avila, J. M., Mendes, C. R. B., et al. (2018). Carbonate system properties in the Gerlache Strait, Northern Antarctic Peninsula (February 2015): II. *Anthropogenic CO_2 Seawater Acidification Deep-Sea Res. Pt. II* 149, 182–192. doi: 10.1016/j.dsr2.2017.07.007

Khatiwala, S., Tanhua, T., Mikaloff Fletcher, S., Gerber, M., Doney, S. C., Graven, H. D., et al. (2013). Global ocean storage of anthropogenic carbon. *Biogeosciences* 10 (4), 2169–2191. doi: 10.5194/bg-10-2169-2013

Kirchman, D., K'nees, E., and Hodson, R. (1985). Leucine incorporation and its potential as a measure of protein synthesis by bacteria in natural aquatic systems. *Appl. Environ. Microbiol.* 49, 599–607. doi: 10.1128/aem.49.3.599-607.1985

Krasakopoulou, E., Souvermezoglou, E., Giannoudi, L., and Goyet, C. (2017). Carbonate system parameters and anthropogenic CO_2 in the North Aegean Sea during october 2013. *Cont. Shelf Res.* 149 (1–13), 69–81. doi: 10.1016/j.csr.2017.04.002

Krasakopoulou, E., Souvermezoglou, E., and Goyet, C. (2011). Anthropogenic CO_2 fluxes in the Otranto Strait (E. Mediterranean) in february 1995. *Deep-Sea Res. I* 58, 1103–1114. doi: 10.1016/j.dsr.2011.08.008

Kropuenske, L. R., Mills, M. M., van Dijken, G. L., Bailey, S., Robinson, D. H., et al. (2009). Photophysiology in two major Southern Ocean phytoplankton taxa: photoprotection in *Phaeocystis* Antarctica and *Fragilariopsis* cylindrus. *Limnol. Oceanogr.* 54, 1176–1196. doi: 10.4319/lo.2009.54.4.1176

Lee, S., Hwang, J., Ducklow, H. W., Hahm, D., Lee, S. H., Kim, D., et al. (2017). Evidence of minimal carbon sequestration in the productive Amundsen Sea polynya. *Geophys. Res. Lett.* 44, 7892–7899. doi: 10.1002/2017GL074646

Lee, K., Kim, T. W., Byrne, R. H., Millero, F. J., Feely, R. A., and Liu, Y. M. (2010). The universal ratio of boron to chlorinity for the North Pacific and North Atlantic Oceans. *Geochim. Et. Cosmochim. Acta* 74 (6), 1801–1811. doi: 10.1016/j.gca.2009.12.027

Legge, O. J., Bakker, D. C. E., Meredith, M. P., Venables, H. J., Brown, P. J., Jones, E. M., et al. (2017). The seasonal cycle of carbonate system processes in Ryder Bay, West Antarctic Peninsula. *Deep Sea Res. Part II: Topical Stud. Oceanogr.* 139, 167–180. doi: 10.1016/j.dsr2.2016.11.006

Lencina-Avila, J. M., Goyet, C., Kerr, R., Orselli, I. B., Mata, M. M., and Touratier, F. (2018). Past and future evolution of the marine carbonate system in a coastal zone of the Northern Antarctic Peninsula. *Deep Sea Res. Part II: Topical Stud. Oceanogr.* 149, 193–205. doi: 10.1016/j.dsr2.2017.10.018

Lenton, A., Tilbrook, B., Law, R. M., Bakker, D., Doney, S. C., Gruber, N., et al. (2013). Sea-air CO_2 fluxes in the Southern Ocean for the period 1990-2009. *Biogeosciences* 10 (6), 4037–4054. doi: 10.5194/bg-10-4037-2013

Lo Monaco, C., Goyet, C., Metzl, N., Poisson, A., and Touratier, F. (2005). Distribution and inventory of anthropogenic CO_2 in the Southern Ocean: Comparison of three data– based methods. *J. Geophys. Res.: Oceans* 110, 1–18, doi: 10.1029/2004JC002643, 2005a.

Loose, B., McGillis, W. R., Perovich, D., Zappa, C. J., and Schlosser, P. (2014). A parameter model of gas exchange for the seasonal sea ice zone. *Ocean Sci.* 10 (1), 17–28. doi: 10.5194/os-10-17-2014

Lorrain, A., Savoye, N., Chauvaud, L., Paulet, Y. M., and Naulet, N. (2003). Decarbonation and preservation method for the analysis of organic C and N contents and stable isotope ratio of low-carbonated suspended particulate material. *Analytica Chimica Acta* 491, 125–133. doi: 10.1016/S0003-2670(03)00815-8

Mahieu, L., Lo Monaco, C., Metzl, N., Fin, J., and Mignon, C. (2020). Variability and stability of anthropogenic CO 2 in Antarctic bottom water observed in the Indian sector of the Southern Ocean 1978–2018. *Ocean Sci.* 16 (6), 1559–1576. doi: 10.5194/os-16-1559-2020

Manna, V., Malfatti, F., Banchi, E., Cerino, F., De Pascale, F., Franzo, A., et al. (2020). Prokaryotic response to phytodetritus-derived organic material in epi-and mesopelagic antarctic waters. *Front. Microbiol.*, 1242. doi: 10.3389/fmicb.2020.01242

Matear, R. J., and Hirst, A. C. (1999). Climate change feedback on the future oceanic CO_2 uptake. *Tellus B* 51 (3), 722–733. doi: 10.3402/tellusb.v51i3.16472

Matsuoka, K., Skoglund, A., and Roth, G. (2018). *QuAntarctica [Data set]* (Norwegian Polar Institute). doi: 10.21334/npolar.2018.8516e961

McKinley, G. A., Fay, A. R., Lovenduski, N. S., and Pilcher, D. J. (2017). Natural variability and anthropogenic trends in the ocean carbon sink. *Annu. Rev. Mar. Sci.* 9, 125–150. doi: 10.1146/annurev-marine-010816-060529

Millero, F. J. (2007). The marine inorganic carbon cycle. *Chem. Rev.* 107, 308–341. doi: 10.1021/cr0503557

Monteiro, T., Kerr, R., Orselli, I. B., and Lencina-Avila, J. M. (2020). Towards an intensified summer CO_2 sink behaviour in the Southern Ocean coastal regions. *Prog. Oceanogr.* 183, 102267. doi: 10.1016/j.pocean.2020.102267

Mu, L., Stammerjohn, S. E., Lowry, K. E., and Yager, P. L. (2014). Spatial variability of surface pCO_2 and air-sea CO_2 flux in the Amundsen Sea Polynya. *Antarctica. Elem. Sci. Anthr.* 2, 000036. doi: 10.12952/journal.elementa.000036

Nelson, D. M., and Smith, W. O.Jr (1991). Sverdrup revisited: critical depth, maximum chlorophyll levels, and the control of Southern Ocean productivity by the irradiance-mixing regime. *Limnol. Oceanogr.* 36, 1650–1661. doi: 10.4319/lo.1991.36.8.1650

Orselli, I. B., Kerr, R., Ito, R. G., Tavano, V. M., Mendes, C. R. B., and Garcia, C. A. (2018). How fast is the Patagonian shelf-break acidifying? *J. Mar. Syst.* 178, 1–14. doi: 10.1016/j.jmarsys.2017.10.007

Orsi, A. H., Johnson, G. C., and Bullister, J. L. (1999). Circulation, mixing, and production of antarctic bottom water. *Prog. Oceanogr.* 43 (1), 55–109. doi: 10.1016/S0079-6611(99)00004-X

Orsi, A. H., and Wiederwohl, C. L. (2009). A recount of Ross Sea waters. *Deep-Sea Res. II Top. Stud. Oceanogr.* 56 (13–14), 778–795. doi: 10.1016/j.dsr2.2008.10.033

Outdot, C., Gerard, R., and Morin, P. (1988). Precise shipboard determination of dissolved oxygen (Winkler procedure) for productivity studies with commercial system. *Limnol. Oceanogr.* 33, 146–150. doi: 10.4319/lo.1988.33.1.0146

Palmiéri, J., Orr, J. C., Dutay, J. C., Béranger, K., Schneider, A., Beuvier, J., et al. (2015). Simulated anthropogenic CO_2 uptake and acidification of the Mediterranean Sea. *Biogeosciences* 12, 781–802. doi: 10.5194/bg-12-781-2015

Pardo, P. C., Pérez, F. F., Khatiwala, S., and Ríos, A. F. (2014). Anthropogenic CO_2 estimates in the Southern Ocean: Storage partitioning in the different water masses. *Prog. Oceanogr.* 120, 230–242. doi: 10.1016/j.pocean.2013.09.005

Pella, E., and Colombo, B. (1973). Study of carbon, hydrogen and nitrogen determination by combustion-gas chromatography. *Mikrochimica Acta* 5, 697–719. doi: 10.1007/BF01218130

Plattner, G. K., Joos, F., Stocker, T. F., and Marchal, O. (2001). Feedback mechanisms and sensitivities of ocean carbon uptake under global warming. *Tellus B: Chem. Phys. Meteorol.* 53 (5), 564–592. doi: 10.3402/tellusb.v53i5.16637

Porter, K. G., and Feig, Y. S. (1980). The use of DAPI for identifying and counting aquatic microflora. *Limnol. Oceanogr.* 25 (5), 943–948. doi: 10.4319/lo.1980.25.5.0943

Porter, D. F., Springer, S. R., Padman, L., Fricker, H. A., Tinto, K. J., Riser, S. C., et al. (2019). Evolution of the seasonal surface mixed layer of the Ross Sea, Antarctica, observed with autonomous profiling floats. *J. Geophys. Res.: Oceans* 124 (7), 4934–4953. doi: 10.1029/2018JC014683

Pritchard, H., Ligtenberg, S. R., Fricker, H. A., Vaughan, D. G., van den Broeke, M. R., and Padman, L. (2012). Antarctic ice-sheet loss driven by basal melting of ice shelves. *Nature* 484 (7395), 502–505. doi: 10.1038/nature10968

Rignot, E., and Jacobs, S. S. (2002). Rapid bottom melting widespread near antarctic ice sheet grounding lines. *Science* 296 (5575), 2020–2023. doi: 10.1126/science.1070942

Ríos, A. F., Vázquez-Rodríguez, M., Padín, X. A., and Pérez, F. F. (2010). Anthropogenic carbon dioxide in the south atlantic western basin. *J. Mar. Syst.* 83 (1-2), 38–44. doi: 10.1016/j.jmarsys.2010.06.010

Rivaro, P., Ianni, C., Langone, L., Ori, C., Aulicino, G., Cotroneo, Y., et al. (2017). Physical and biological forcing of mesoscale variability in the carbonate system of the Ross Sea (Antarctica) during summer 2014. *J. Mar. Syst.* 166, 144–158. doi: 10.1016/j.jmarsys.2015.11.002

Rivaro, P., Ianni, C., Raimondi, L., Manno, C., Sandrini, S., Castagno, P., et al. (2019). Analysis of physical and biogeochemical control mechanisms on summertime surface carbonate system variability in the Western Ross Sea (Antarctica) using *in situ* and satellite data. *Remote Sens.* 11 (3), 238. doi: 10.3390/rs11030238

Rivaro, P., Messa, R., Ianni, C., Magi, E., and Budillon, G. (2014). Distribution of total alkalinity and pH in the Ross Sea (Antarctica) waters during austral summer 2008. *Polar Res.* 33, 269. doi: 10.3402/polar.v33.20403

Roden, N. P., Shadwick, E. H., Tilbrook, B., and Trull, T. W. (2013). Annual cycle of carbonate chemistry and decadal change in coastal Prydz Bay, East Antarctica. *Mar. Chem.* 155, 135–147. doi: 10.1016/j.marchem.2013.06.006

Roden, N. P., Tilbrook, B., Trull, T. W., Virtue, P., and Williams, G. D. (2016). Carbon cycling dynamics in the seasonal sea-ice zone of East Antarctica. *J. Geophys. Res.: Oceans* 121, 8749–8769. doi: 10.1002/2016JC012008

Rysgaard, S., Bendtsen, J., Pedersen, L. T., Ramløv, H., and Glud, R. N. (2009). Increased CO_2 uptake due to sea ice growth and decay in the Nordic Seas. *J. Geophys. Res.: Oceans* 114 (C9), C09011. doi: 10.1029/2008jc005088

Rysgaard, S., Glud, R. N., Lennert, K., Cooper, M., Halden, N., Leakey, R. J. G., et al. (2012). Ikaite crystals in melting sea ice implications for pCO_2 and pH levels in Arctic surface waters. *Cryosphere* 6, 901–908. doi: 10.5194/tc-6-901-2012

Rysgaard, S., Glud, R. N., Sejr, M. K., Bendtsen, J., and Christensen, P. B. (2007). Inorganic carbon transport during sea ice growth and decay: A carbon pump in polar seas. *J. Geophys. Res. Oceans* 112, C03016. doi: 10.1029/2006JC003572

Sabine, C. L., Feely, R. A., Gruber, N., Key, R. M., Lee, K., Bullister, J. L., et al. (2004). The oceanic sink for anthropogenic CO_2. *Science* 305, 367–371. doi: 10.1126/science.1097403

Sabine, C. L., and Tanhua, T. (2010). Estimation of anthropogenic CO_2 inventories in the ocean. *Annu. Rev. Mar. Sci.* 2, 175–198. doi: 10.1146/annurev-marine-120308-080947

Saggiomo, V., Catalano, G., Mangoni, O., Budillon, G., and Carrada, G. C. (2002). Primary production processes in ice-free waters of the Ross Sea (Antarctica) during the austral summer 1996. *Deep Sea Res. Part II: Topical Stud. Oceanogr.* 49 (9-10), 1787–1801. doi: 10.1016/S0967-0645(02)00012-7

Sakshaug, E., Slagstad, D., and Holm-Hansen, O. (1991). Factors controlling the development of phytoplankton blooms in the antarctic ocean – a mathematical model. *Mar. Chem.* 35, 259–271. doi: 10.1016/S0304-4203(09)90021-4

Sambrotto, R. N., Matsuda, A., Vaillancourt, R., Brown, M., Langdon, C., Jacobs, S. S., et al. (2003). Summer plankton production and nutrient consumption patterns in the Mertz Glacier Region of east Antarctica. *Deep-Sea Res. Part II: Topical Stud. Oceanogr.* 50 (8–9), 1393–1414. doi: 10.1016/S0967-0645(03)00076-6

Sandrini, S., Ait-Ameur, N., Rivaro, P., Massolo, S., Touratier, F., Tositti, L., et al. (2007). Anthropogenic carbon distribution in the Ross Sea, Antarctica. *Antarctic Sci.* 19 (3), 395–407. doi: 10.1017/S0954102007000405

Sedwick, P. N., DiTullio, G. R., and Mackey, D. J. (2000). Iron and manganese in the Ross Sea, Antarctica: Seasonal iron limitation in antarctic shelf waters. *J. Geophys. Res.: Oceans* 105 (C5), 11321–11336. doi: 10.1029/2000JC000256

Sedwick, P. N., Marsay, C. M., Sohst, B. M., Aguilar-Islas, A. M., Lohan, M. C., Long, M. C., et al. (2011). Early season depletion of dissolved iron in the Ross Sea polynya: Implications for iron dynamics on the antarctic continental shelf. *J. Geophys. Res.: Oceans* 116, C12019. doi: 10.1029/2010JC006553

Shadwick, E. H., Tilbrook, B., and Currie, K. I. (2017). Late-summer biogeochemistry in the Mertz Polynya: East Antarctica. *J. Geophys. Res. Oceans* 122, 7380–7394. doi: 10.1002/2017JC013015

Shadwick, E. H., Tilbrook, B., and Williams, G. D. (2014). Carbonate chemistry in the mertz polynya (East Antarctica): Biological and physical modification of dense water outflows and the export of anthropogenic CO_2. *J. Geophys. Res. Oceans* 119, 1–14. doi: 10.1002/2013JC009286

Sharp, J. H. (1974). Improved analysis for particulate organic carbon and nitrogen from seawater. *Limnol. Oceanogr.* 19 (6), 984–989. doi: 10.4319/lo.1974.19.6.0984

Sigman, D. M., Hain, M. P., and Haug, G. H. (2010). The polar ocean and glacial cycles in atmospheric CO_2 concentration. *Nature* 466 (7302), 47–55. doi: 10.1038/nature09149

Smith, D. C., and Azam, F. (1992). A simple, economical method for measuring bacterial protein synthesis rates in sea water using ^{3}H-leucine. *Mar. Microbial. Food Webs* 6, 107–114.

Smith, W. O., and Gordon, L. I. (1997). Hyperproductivity of the Ross Sea (Antarctica) polynya during austral spring. *Geophys. Res. Lett.* 24, 233–236. doi: 10.1029/96GL03926

Smith, W. O.Jr., Marra, J., Hiscock, M. R., and Barber, R. T. (2000). The seasonal cycle of phyto- plankton biomass and primary productivity in the Ross Sea, Antarctica. *Deep-Sea Res. II* 47, 3119–3140. doi: 10.1016/S0967-0645(00)00061-8

Smith, W. O.Jr., Sedwick, P. N., Arrigo, K. R., Ainley, D. G., and Orsi, A. H. (2012). The Ross Sea in a sea of change. *Oceanography* 25 (3), 90–103. doi: 10.5670/oceanog.2012.80

Smith, W. O.Jr., Shields, A. R., Peloquin, J. A., Catalano, G., Tozzi, S., Dinniman, M. S., et al. (2006). Interannual variations in nutrients, net community production, and biogeochemical cycles in the Ross Sea. *Deep Sea Res. Part II: Topical Stud. Oceanogr.* 53 (8-10), 815–833. doi: 10.1016/j.dsr2.2006.02.014

Sulpis, O., Lauvset, S. K., and Hagens, M. (2020). Current estimates of k 1* and k 2* appear inconsistent with measured CO_2 system parameters in cold oceanic regions. *Ocean Sci.* 16 (4), 847–862. doi: 10.5194/os-16-847-2020

Sweeney, C., Smith, W. O.Jr, Hales, B., Bidigare, R. R., Carlson, C. A., Codispoti, L. A., et al. (2000). Nutrient and carbon removal ratios and fluxes in the Ross Sea, Antarctica. *Deep-Sea Res. II* 47, 3395–3421. doi: 10.1016/S0967-0645(00)00073-4

Takahashi, T., Sweeney, C., Hales, B., Chipman, D., Newberger, T., Goddard, J., et al. (2012). The changing carbon cycle in the Southern Ocean. *Oceanogr.* 25, 26–37. doi: 10.5670/oceanog.2012.71

Thyng, K. M., Greene, C. A., Hetland, R. D., Zimmerle, H. M., and DiMarco, S. F. (2016). True colors of oceanography: Guidelines for effective and accurate colormap selection. *Oceanography* 29 (3), 9–13. doi: 10.5670/oceanog.2016.66

Touratier, F., Azouzi, L., and Goyet, C. (2007). CFC-11, $\Delta C^{14}C$ and 3^H tracers as a means to assess anthropogenic CO_2 concentrations in the ocean. *Tellus* 59B, 318–325. doi: 10.1111/j.1600-0889.2006.00247.x

Touratier, F., and Goyet, C. (2004a). Definition, properties, and atlantic ocean distribution of the new tracer TrOCA. *J. Mar. Syst.* 46, 169–179. doi: 10.1016/j.jmarsys.2003.11.016

Touratier, F., and Goyet, C. (2004b). Applying the new TrOCA approach to assess the distribution of anthropogenic CO_2 in the atlantic ocean. *J. Mar. Syst.* 46, 181–197. doi: 10.1016/j.jmarsys.2003.11.020

Touratier, F., Goyet, C., and Coatanoan, C. (2005). Assessments of anthropogenic CO_2 distribution in the tropical atlantic ocean. *Deep-Sea Res. I Vol.* 52, 2275–2284. doi: 10.1016/j.dsr.2005.09.001

Touratier, F., Goyet, C., Houpert, L., De Madron, X. D., Lefèvre, D., Stabholz, M., et al. (2016). Role of deep convection on anthropogenic CO_2 sequestration in the Gulf of Lions (Northwestern Mediterranean Sea). *Deep Sea Res. Part I: Oceanogr. Res. Pap.* 113, 33–48. doi: 10.1016/j.dsr.2016.04.003

Vázquez-Rodríguez,, Touratier, F., Lo Monaco, C., Waugh, D. W., Padin, X. A., Bellerby, R. G. J., et al. (2009). Anthropogenic carbon distributions in the atlantic ocean: data-based estimates from the Arctic to the Antarctic. *Biogeosciences* 6, 439–451. doi: 10.5194/bg-6-439-2009

Wang, Q., Danilov, S., Hellmer, H. H., Sidorenko, D., Schröter, J., and Jung, T. (2013). Enhanced cross-shelf exchange by tides in the Western Ross Sea. *Geophys. Res. Lett.* 40, 5735–5739. doi: 10.1002/2013GL058207

Whitworth, T., and Orsi, A. H. (2006). Antarctic bottom water production and export by tides in the Ross Sea. *Geophys. Res. Lett.* 33 (12), L12609. doi: 10.1029/2006GL026357

Williams, W. J., Carmack, E. C., and Ingram, R. G. (2007). Physical oceanography of polynyas. *Elsevier Oceanogr. Ser.* 74, 55–85. doi: 10.1016/S0422-9894(06)74002-8

Yool, A., Oschlies, A., Nurser, A. J. G., and Gruber, N. (2010). A model-based assessment of the TrOCA approach for estimating anthropogenic carbon in the ocean. *Biogeosciences* 7 (2), 723–751. doi: 10.5194/bg-7-723-2010